9121573

LIBRARY
Michigan State
University

This is to certify that the
thesis entitled

Parametric Material Layout Optimization of Natural Fiber
Composite Panels

presented by

Christina Isaac

has been accepted towards fulfillment
of the requirements for the

M.S. degree in Mechanical Engineering

Major Professor's Signature

8/23/05

Date

MSU is an Affirmative Action/Equal Opportunity Institution

PLACE IN RETURN BOX to remove this checkout from your record.
TO AVOID FINES return on or before date due.
MAY BE RECALLED with earlier due date if requested.

DATE DUE	DATE DUE	DATE DUE

6/01 c:/CIRC/DateDue.p65-p.15

PARAMETRIC MATERIAL LAYOUT OPTIMIZATION OF NATURAL FIBER COMPOSITE PANELS

By

Christina Isaac

A THESIS

Submitted to
Michigan State University
in partial fulfillment of the requirements
for the degree of

MASTER OF SCIENCE

Department of Mechanical Engineering

2005

ABSTRACT

MATERIAL LAYOUT OPTIMIZATION OF NATURAL FIBER COMPOSITE PANELS

By

Christina Isaac

Natural fiber composites, have recently gained renewed interest due to increased concern for the long-term sustainability of structural materials. Nonetheless, their use for load-bearing applications has been restricted because of their low mechanical properties. Yet, recent developments have shown that the performance of biocomposite components can be overcome by using properly engineered or optimized designs.

This thesis presents a finite, parametric approach to optimize the material distribution in biocomposite cellular panels. The approach combines optimization and finite-element software through a parametric problem formulation. Unlike traditional topology optimization, the presented approach leads to optimized material layouts while permitting the use of multiple objectives and constraints. The optimization procedure was validated using benchmark topology problems. Small-scale component testing was conducted to validate the optimized solutions and evaluate the vacuum assisted resin transfer molding as a method to create the optimized biocomposite cellular panels.

The parametric optimization results compared favorably to the multi-resolution topology solutions and lead to designs that are easier to manufacture than those obtained by the power-law method. As expected, the manufactured optimized designs exhibited improved performance. Thus, the material layout optimization technique implemented for this study has proven to be viable for achieving optimal structural layouts to enhance the performance of biocomposites while simultaneously accounting for manufacturing.

Copyright by

Christina Isaac

2005

To my parents, Sam and Rema Isaac, my sister, Marie, and brothers, Danny and Jacob for all of their love, support, and guidance throughout the years

ACKNOWLEDGEMENTS

I am most thankful for my advisor Dr. Rigoberto Burgueño, for his support, patience, and guidance, throughout this research. His time, dedication, and encouragement provided me with the knowledge and strength to become successful in my research as well as my future aspirations. The topic and ideas presented throughout this thesis were proposed by him.

I would also like to acknowledge the members of my graduate committee, Dr. Ronald Averill and Dr. Alejandro Diaz for their interest, and insightful ideas throughout my research.

I am also very grateful for the guidance and support offered by Dr. Amar Mohanty, Dr. Manjusri Mirsa, and Dr. Hiro Miyagawa. They expertise in biocomposites provided me with assistance to progress in my work. Furthermore, I would like to thank them for providing me with necessary supplies needed for manufacturing of my cellular biocomposite samples.

I would like to thank Siavosh Ravanbakhsh for his help with fabrication and testing of biocomposite cellular samples at the Civil Infrastructure Laboratory. He was always willing to assist and to provide insight and encouragement when needed.

I am also grateful for the assistance of Robert Jurek for his advice and expertise with the vacuum assisted resin transfer molding (VARTM) manufacturing process and for providing me with VARTM materials when needed.

I am also very appreciative of the staff at Red Cedar Technology for training me on and providing me with effective optimization software to implement in my research.

Lastly, I wish to thank all my colleagues for their assistance, and most importantly their friendship throughout my years of graduate school at MSU. Their encouragement helped me get through the all difficult times in my research.

TABLE OF CONTENTS

LIST OF TABLES

LIST OF FIGURES

1 INTRODUCTION

1.1 Overview

Increased environmental awareness and interest in long-term sustainability of structural materials have recently challenged the development of environmentally friendly alternatives to fiber reinforced polymer (FRP) composites (Mohanty et al. 2000). FRP composites provide advantages such as high stiffness and strength to weight ratios in comparison to conventional construction materials; however, due to their high initial material costs, restricted use in efficient structural forms, and environmental impact, their application for structural components has been limited (Burgueño et al. 2004).

Natural fiber reinforced polymer composites, or biocomposites, have been gaining renewed interest as an environmentally friendly alternative to synthetic FRP composites and have become appealing for diverse applications for reasons which also include low cost and light weight. Despite these advantages, their main disadvantage is that their mechanical properties, such as strength and stiffness, are much lower than those of synthetic FRP composites and other conventional structural materials, which do not seem to make them useful for load-bearing applications. However, recent studies have shown that through proper engineering and processing, biocomposites are capable of competing with E-glass FRP composites (Mohanty et al. 2000).

The performance of a component depends on both its material and structural properties. The lower material stiffness biocomposite materials can be thus overcome using properly engineered structural configurations that place material in specific locations to achieve the highest structural performance while using minimum material (Gibson and Ashby 1988). This idea of has been recently gaining much attention due to renewed interest and knowledge into the way nature uses materials to achieve complex structural configurations for adequate structural efficiency.

The concepts introduced throughout this section have been integrated into this research to display that properly engineered biocomposites can serve as environmentally friendly, cost-effective, and adequate load bearing components. The remaining sections of this chapter will give a general overview of the research objectives, followed by the background information which motivated these objectives. The background incorporates an introduction and discussion of natural fiber composites, material structures in biology, numerical methods that are capable of achieving strategic material layouts, and manufacturing limitations. The chapter is concluded with the specific research objectives and scope of the research work presented in this thesis.

1.2 General Research Objective

The objective of this research was to explore and implement an optimization technique to improve the performance of natural fiber reinforced polymer composites (biocomposites) for load-bearing applications. The optimization procedure was validated using benchmark data from well-accepted optimization techniques and design solutions were validated through small-scale component testing.

The research work involved the following tasks:

- Development and implementation of the optimization procedure
- Validation of the optimization procedure

- Manufacturing of designs solutions
- Experimental validation and analysis

A general description of the objectives was outlined prior to providing a background on this study to display the direction of this research at the onset. Specific objectives will be outline in greater detail in a later section in this chapter.

1.3 Natural Fiber Composites

Natural fibers have recently gained much attention for reasons including low cost, lightweight, increased environmental awareness, interest in long term sustainability, and for their ability to compete with glass fiber composites (Mohanty et al. 2000, Burgueño et al. 2004) Types of common natural fibers include sisal, henequen, flax, hemp, jute, kenaf, cotton, and coir (coconut husk). The quality of the fiber depends highly on size, maturity, processing method used for fiber extraction, and origin of the fiber. Depending on the origin, biofibers can be grouped into one of the following categories: leaf, bast, seed, or fruit. Examples of each include: leaf: sisal and henequen, bast: flax, hemp, kenaf, and jute, seed: cotton and fruit: coconut husk (coir), (Mohanty et al. 2000) (Figure 1-1).

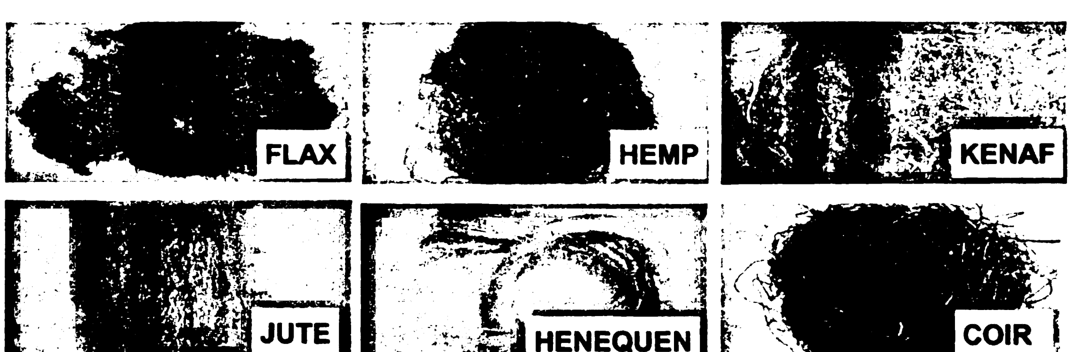

Figure 1-1. Examples of natural fibers

Natural fibers have two basic components: cellulose and lignin. These two constituents work to provide rigidity to the walls of plants stems and also the bonding in between them. The contents of both cellulose and lignin vary from one natural fiber to another.

The density of natural fibers is relatively low in comparison to that of synthetic composites, such as E-glass, thus, it can be shown that the bast fibers (e.g. flax, hemp, and jute) have specific strengths, elastic modulus, and specific modulus that are comparable or even superior to E-glass (Mohanty et al. 2000) (Table 1-1). Other advantages include, ease of separation and enhanced energy recovery. Due to their acceptable properties and numerous environmental advantages, natural fibers have attracted renewed interest as a glass fiber substitute in a variety of industries.

Table 1-1. Basic fiber properties (Lackey et al. 2004)

Property	E-Glass	Flax	Hemp	Jute
Density (lbs/in^3)	0.092	0.050	0.053	0.052
Tensile Strength (ksi)	348	116-217.5	79.7-130.5	58-116
E-Modulus (ksi)	1.06E+04	8.70E+03- 1.20E+03	1.00E+04	1.50E+03 - 4.40E+03
Specific Modulus (E/Density)	1.15E+05	1.74E+05 - 2.40E+05	1.89E+05	2.88E+04 - 8.46E+04
Moisture Absorption (%)	--	7	8	12
Cost ($/lb) Raw	0.59	0.23-0.68	0.27-0.81	0.16

Although natural fibers possess sufficient strength and stiffness, and have environmental qualities that make them attractive over synthetic composites, they also have several major drawbacks. Among the most relevant drawbacks are that natural fibers tend to be highly moisture absorbent, generally need to be processed under low temperatures to reduce the possibility of fiber degradation, and have extremely low tolerance to processing damage (Rout et al. 2001). Manufacturing limitations are also important due to the "springy" nature of the fibers, their cotton-like texture, and extreme randomness, i.e. varying shapes and sizes. Natural fibers tend to clump together and should be separated prior to manufacturing to ensure uniform dispersion throughout the composite. Furthermore, since they are "fluffy" and possess a cotton-like texture, it is suggested that they remain compressed throughout manufacturing (Brouwer 2000). By compressing the fibers, the natural adhesive lignin is released thus forming a slight bond between fibers. This bond assists in preventing the fibers from shifting during manufacturing and may also help in maintaining uniform distribution throughout the composite. If the compression of these fibers is accomplished through automated processing, the mechanical properties of the fibers could decrease due high temperatures and possible chemical and/or physical treatments (Hepworth et al. 2000). Therefore, natural fiber composites are typically manufactured through hand-lay procedures or by vacuum assisted resin transfer molding (VARTM) depending on geometric complexity.

1.4 Material Structures in Biology

Nature has displayed that through proper combination of natural constituents in advanced geometries, adequate structural efficiency can be achieved even when the raw constituents have rather low individual properties. Engineers are beginning to take advantage of this knowledge and are attempting to mimic nature with intentions of developing materials that may be useful for various structural applications. The study of natural materials has also introduced advanced engineering forms at the material and structural levels (Srinivasan 1995). For example, materials of living organisms, such as tendons and bones, which possess unique hierarchical structural forms that provide them with increased toughness and ductility. The rope was the first application to mimic these natural materials and has proved to be applicable in various structural components (Srinivasan 1995). Wood is another example of a natural composite that exhibits a remarkable combination of strength, stiffness, and toughness (Srinivasan 1995). It is comprised of parallel columns of hollow cells joined end-to-end, around which fibers of cellulose are wound in spirals and embedded to a matrix of lignin, a natural adhesive. The structural formation of wood (Figure 1-2), together with its material constituents provides this material with the capability to absorb large amounts of energy. When a wood cell buckles inward, it fractures the surrounding cells, absorbing energy in the process. A long spiral crack develops along the wound fibers, dissipating energy over a short length of the wood. Since the crack runs along and in between the fibers and within the lignin, the fibers are able to stay intact so that the macroscopic wood material will not fall apart. Even though the overall wood material is fractured, it is still capable of supporting load (Srinivasan 1995, Hepworth et al. 2000)

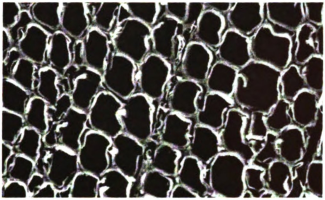

Figure 1-2. Transverse view of wood cellular structure

Natural materials do have various disadvantages that limit their use. As stated previously, natural fibers easily absorb excess moisture, causing swelling and degradation. They also have limited processing temperatures due to degradation and flammability. Natural fibers, or biofibers, have variable quality depending on origin and weather influences. They have irregular lengths, shapes, and sizes, which makes them difficult to handle and manufacture (Verheus 2002). The major limitations of natural fibers are their low mechanical properties, such as strength and stiffness, which restricts their use to non load-bearing applications. However, nature elegantly shows that materials with low mechanical properties can be enhanced through hybrid formations and strategic material organization such as complex hierarchical configurations. Biofibers are extremely fibrous and therefore can be easily combined with synthetic fibers, such as carbon, glass, nylon, polyester and/or polyethylene to form hybrid designs. Furthermore, complex hierarchical configurations seem appropriate for biocomposites due to the complexity in manufacturing pieces with aligned reinforcement, which suggests their use as a continuous distributed material (Burgueño et al. 2005). By combination of advanced structural forms and hybrid designs a more enhanced structural material with higher performance can be achieved, while simultaneously minimizing cost and weight (Allinger et al. 1996).

Previous research on biocomposites for structural applications has considered analytical and experimental evaluations of the mechanical properties of various natural fiber laminates and cellular structures (Burgueño et al. 2004, Burgueño et al. 2005, Quagliata 2003). The research concluded that biocomposites in cellular/sandwich structures are capable of serving as load bearing components and are able to compete with conventional structural materials. In general, this work has shown that by altering the material layout of a structure, strategic arrangements or hierarchical forms can effectively improve the mechanical properties of biocomposites thus making them competitive for load-bearing applications.

1.5 Achieving Strategic Material Layouts

In order to achieve strategic material layouts to improve the mechanical properties of biocomposites, without going through the trial and error of experimentation and when solutions might be non-intuitive, engineers use structural optimization algorithms. Optimization algorithms are now feasible due to diverse computational tools which allow for modeling and analysis of complex shapes and internal geometries for better understanding of the performance of various structural layouts (Bendsöe and Sigmund 2003).

Structural optimization is employed to improve the performance of a design, e.g. maximizing stiffness or minimizing weight. An objective function is used to locate a solution by measuring the "fitness" or efficiency of each design. Optimization problems are typically formulated with limitations or constraints such as maximum and minimum stresses, strains, and deflections that control the design selection (Arora 1989). Various optimization algorithms exist which can be combined with the use of finite element software to perform structural optimization techniques that are capable of optimizing a structure's topology, size, and/or shape (Arora 1989, Haftka and Gurdal 1993). Topology optimization is typically employed to determine the material arrangement, or layout, within a structure in a way that will allow it to serve in its the most efficient manner. Size optimization generally focuses on achieving an optimal cross-sectional area, typically centering on obtaining an optimal shape of the domain or internal geometry (Haftka and Gurdal 1993). It should be noted that while designs obtained through optimization techniques may be optimal they are not always feasible, or cost-effective, to manufacture. This can be particularly important when using natural fibers, as discussed next.

1.6 Manufacturing Limitations

Designs obtained through the use of structural optimization techniques can be rather intricate and difficult to manufacture using natural fibers; therefore significant post-processing techniques may be required to simplify the geometry of the optimal design solutions to ensure manufacturability. Rather than relying on post-processing measures, an alternate solution to geometric simplification is to implement an optimization technique which deals with finite and well-defined geometrical changes, eliminating the geometric intricacies that tend to create difficulties in manufacturing with natural fibers. Chellappa et al. (2004) proposed an elegant topology optimization scheme with finite size inclusions using a multiresolution method. This technique is capable of optimizing the material layout within a given domain using a predefined set of inclusions, therefore minimizing the need for rigorous post-processing prior to manufacturing. This technique locates the optimal material layout of a given structure while maximizing stiffness (Chellappa et al. 2004). However, the disadvantage of this method is that it is not designed for ease of problem reformulation. Specifically, altering loading and boundary conditions, incorporating system constraints, i.e. stresses, strains, and deformations, or employing multiple objective functions would require code restructuring. Thus, in order to account for manufacturing and redefining system conditions and constraints, it is necessary to develop and implement an optimization procedure with finite resolution that also minimizes the complexities of problem reformulation. Such a technique would allow multiple constraints and objective functions to be incorporated into the design optimization problems with ease.

1.7 Parametric Layout Optimization

Due to the limitation of the multiresolution technique proposed by Chellappa et al. 2004 (see Section 1-6), an alternate optimization procedure was explored to perform material layout optimization for the present work. A parametric approach to material layout optimization was investigated and implemented. This parametric based optimization technique uses existing finite element software and a general purpose optimization program to optimize the material layout within a structural domain subject to loading and boundary conditions. This technique allows for incorporation of multiple design constraints and objective functions without significant code restructuring and simultaneously accounts for manufacturing.

1.8 Objective and Scope

The objective of this research was to investigate and implement a material layout optimization technique to improve the performance of natural fiber reinforced polymer composites (biocomposites) for load-bearing paneling applications. A material layout topology with finite geometrically defined features was sought due to the known complexities in manufacturing biocomposite panels. This optimization technique was applied in the context of a specific problem, specifically, the material distribution within the transverse cross-section of a continuous panel system. Such a panel system was optimized and optimal design solutions were validated through small-scale component testing. The goal is to develop a design optimization approach that would allow for the use of biocomposites in applications ranging from civil structures (such as bridges, decks, and flooring systems) to aerospace structures (such as fuselages, wing skins, and various other integrated components). As stated previously, the material layout optimization technique should be powerful enough to incorporate multiple objective functions and loading conditions for problems relating to solid mechanics, fluid mechanics, and dynamic/vibration analysis.

The research work involved the following tasks:

- Development and implementation of the parametric material layout optimization technique:
- Validation of the parametric material layout optimization technique
- Manufacturing of optimal designs
- Experimental validation and analysis

The research presented in this thesis incorporates concepts of topology, shape, and material layout optimization techniques; fabrication of natural fiber composite components, and experimental structural testing. All of these concepts are linked through the motivation to improve the feasibility of natural fiber composites for load-bearing applications. A parametric material layout optimization process is introduced and implemented to locate optimal material layouts throughout panel cross-sections that will enhance structural performance. The designs obtained through the developed structural optimization approach are used to validate the use of natural fiber composites for load-bearing applications.

Based on the above research tasks, the chapters of the thesis are organized in the following order:

- Chapter 2: Optimization Background
- Chapter 3: Development and Implementation of Parametric Material Layout Optimization Technique
- Chapter 4: Experimental Validation
- Chapter 5: Conclusions and Recommendations

2 OPTIMIZATION BACKGROUND

2.1 Overview of Structural Optimization

Structural optimization has become a chief concern in the design of mechanical systems, civil infrastructure, and aeronautical and aerospace integrated components. Engineers are no longer satisfied with simple design improvements, but are now striving for structurally efficient design solutions through global optimization of weight, cost, and/or stiffness. Generally, engineers will attempt to improve designs through trial and error, and an optimal solution is found by intuition. The disadvantage of this approach is that it is very costly, time-consuming, and may result in erroneous design solutions (Red Cedar Technology 2004). Therefore, numerical optimization strategies have become very attractive and valuable tools in creating efficient and adequate designs for structural components without encountering the problems introduced by the trial and error approach.

Typical structural optimization problems involve the search for the minimum or maximum value of objective functions subjected to a set of constraints and/or restrictions on the sizes or shapes of structural component members. The constraints are usually dependent on performance measures such as stresses and deflections (Arora 1989, Haftka and Gurdal 1993, Turkkan 2003). Structural optimization becomes even more powerful when combined with computational tools such as finite element software and computer aided design. This combination can assist in creating cost-effective, lightweight structures, while minimizing design time (Haftka and Gurdal 1993). Various optimization techniques exist that are suitable to use when optimizing the material distribution of a structural component and can be categorized by search method or goal (i.e. what is being optimized).

Two common search algorithms exist and include gradient search algorithms and the stochastic search algorithms. The gradient search technique uses information of the first and possibly second order derivatives of the objective function are used to determine an optimal search direction towards the optimum. Information from these derivatives guarantees decreasing values for the objective function in consecutive iterations. The disadvantage of this method is that it is sensitive to the initial estimates of the unknown variables if the objective function has more than one optimum. This means that it is possible for the algorithm to converge to a local optimum instead of the wanted global optimum (Arora 1989). Stochastic search methods, commonly implemented by genetic algorithms (Section 2-2), use randomized decisions while searching for solutions to a given problem. They operate on a population of solutions to locate a global optimum and are less likely to get "stuck" at local optimums, in comparison to gradient search methods. A genetic algorithm will continue to search for optimal solutions until the allotted number of user defined cycles has completed. Convergence can be detected if the fitness value of the last successive designs is relatively close in value, or if the last design found was obtained approximately 10 cycles prior to completion of the last cycle (Arora 1989).

Structural optimization techniques are typically implemented to achieve one of three goals and are categorized in this manner throughout this study. Researchers have proposed ideas such size, shape, and/or topology optimization (Haftka and Gurdal 1993). For example, given a defined domain, Ω, boundary and loading conditions (see Figure 2-1), size optimization generally refers to a change in the cross-sectional area of Ω; shape optimization typically refers to change in shape of the domain, but not the topology; and topology optimization can be implemented to incorporate size and shape optimization as well as the material layout and/or topology within Ω. Note that topology optimization generally does not affect the size of the defined domain (Figure 2-1).

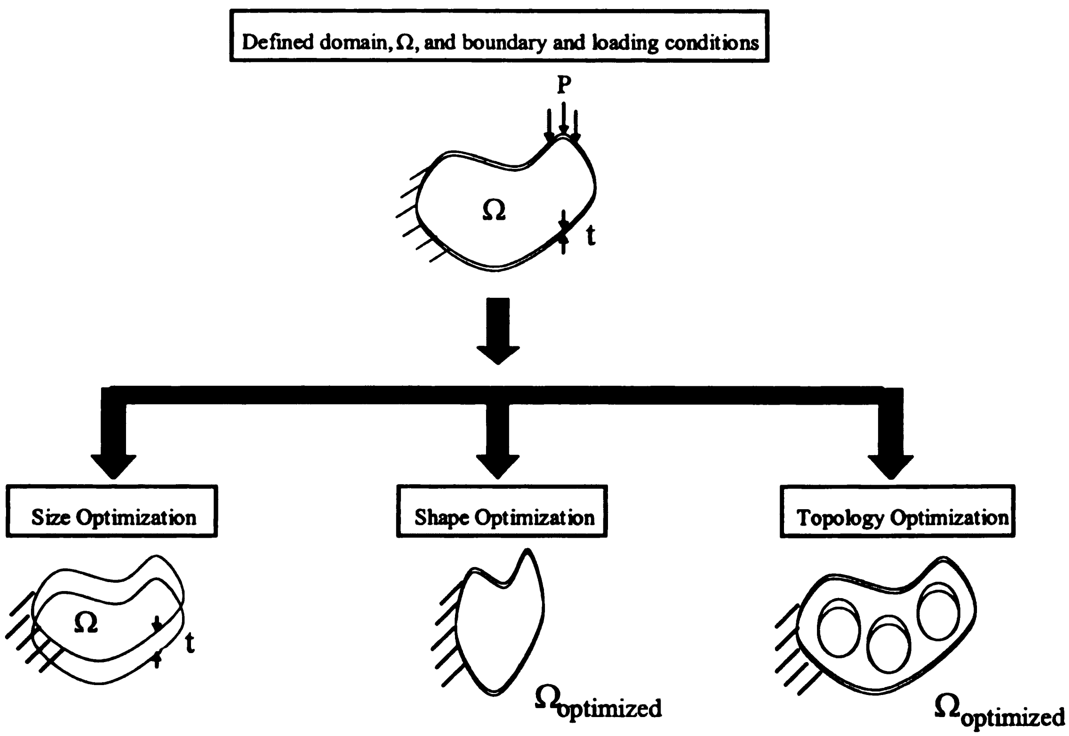

Figure 2-1. Main types of structural optimization techniques

2.1.1 Size and Shape Optimization

Of the three types of structural optimization techniques introduced above, size and shape optimization are the most commonly used. Size optimization is typically concerned with optimization of "sizing variables" such as the thickness or cross-sectional area of a structure, where modification of the cross-section is performed by altering the size of the individual finite elements. This technique is typically implemented to homogenize the stress or strain distribution throughout a structure's cross-section (Haftka and Gurdal 1993, Allinger 1996, Spath et al. 2002)

Shape optimization problems are typically more difficult to solve than size optimization problems. Shape optimization generally refers to two types of problems: (1) optimizing the shape of the boundary of a structural component (either 2 or 3 dimensional) or (2) optimization of the shape of internal cavities or holes. Implementing shape optimization by altering the boundary or domain of a structure is performed by changing the configuration of the structure by creating new boundaries as well as modifying the existing boundaries in the model (Canonaco et al. 1997). These boundaries are generally altered by changing the position of existing nodes or removing nodes in a finite element mesh based on calculated stress levels. The goal is to homogenize the stress distribution according to the specified stress constraint. As the shape of the structure is modified, it is necessary to re-mesh the finite element model, which can lead to element distortion and loss of accuracy in computational solutions (Haftka and Gurdal 1993). This problem is typically addressed through manual re-meshing or through implementation of mesh generators (Haftka and Gurdal 1993).

The optimization of boundaries or holes within a domain can also be defined as shape optimization. This technique has the ability to produce optimal designs with internal cavities; however, these vacancies cannot be generated without prior knowledge of their existence. Specifically, this optimization procedure can easily locate the optimum shape of a cavity once one is assumed, but it cannot determine how many cavities should exist (Haftka and Gurdal 1993). For example, if shape optimization is implemented on a structure with four holes the optimal solution will also have four holes. The positioning and/or size of these holes may differ from those in the original structure, but this technique is incapable of increasing the number of holes, removing holes, or merging them without resorting to specialized post-processing or interpreting algorithms. An example of shape optimization in a cantilever beam subjected to a concentrated load is shown in Figure 2-2.

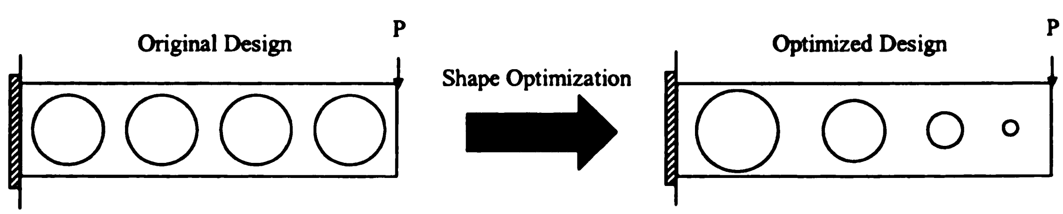

Figure 2-2. Example of shape optimization with internal cavities or holes

A common problem in shape optimization is to optimize the shape of a hole in a plate subjected to a uniform tension field (Figure 2-3) to reduce stress concentrations around the hole (Haftka and Gurdal 1993). The optimization procedure is formulated using the nodes surrounding the hole together with other design parameters. Even though the original shape of the hole may be an adequate design, it may not be the optimal (Haftka and Gurdal 1993). In comparison to the original design (see Figure 2-2), the optimal configuration was designed to homogenize the stress distribution around the hole according to the specified stress constraint.

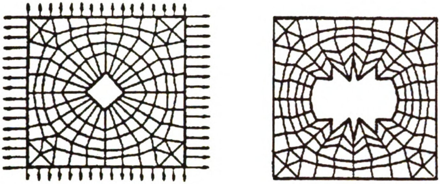

Figure 2-3. Common example used for shape optimization (Taken from [Haftka and Gurdal 1993])

Shape optimization techniques are very robust and have been under improving development for years; however they have limitations with respect to modifying the number of existing cavities in a domain to truly optimize the material distribution within a structure (Haftka and Gurdal 1993). These restrictions led to the development and implementation of an alternate optimization technique for optimal material layout design: topology optimization.

2.1.2 Topology Optimization

Topology optimization is the third commonly implemented structural optimization technique and will be discussed in greater detail because it portrays ideas most closely related to those represented by the parametric material layout optimization approach (see Chapter 3). The goal of topology optimization is to efficiently distribute material throughout a defined structural domain subject to prescribed loading and boundary conditions, such that the stiffness of the structure is maximized (Haftka and Gurdal 1993, Sigmond and Tcherniak 2001, Canonaco et al. 1997). Topology optimization uses finite element formulations to generate optimal design concepts. Given a problem definition consisting of a defined domain, loading and boundary conditions, and mass and deflection constraints, the most structurally efficient material layout can be determined. Initially, the available material is evenly distributed throughout the domain, and then re-distributed within the design space until the structure has achieved adequate stiffness. The redistribution of material is achieved by addition, removal, or merging of cavities within the domain, resulting in an optimal starting point for a refined design (Haftka and Gurdal 1993). Diverse topology optimization techniques have been developed to optimize the material distribution of various structures. Topology optimization algorithms can be extremely robust provided a sufficient problem definition exists (Canonaco et al. 1997). In spite of its power, topology optimization techniques locate optimal solutions (i.e. designs) that feature extensively detailed geometries, which can be difficult to manufacture. If this is the case, shape optimization strategies can be explored to "fine-tune" the design; or a topological algorithm which is capable of preserving efficient and adequate structural designs can be implemented (Canonaco et al. 1997).

The homogenization method is one common method used to implement topology optimization. This idea was introduced by Bendsöe and Kikuchi, and is implemented to optimize the material distribution in a perforated structure with infinite micro-scale voids. This is accomplished by discretizing a specified domain into multiple finite elements where a material density is then prescribed over the defined domain. The optimal density of each element is determined from the stress limit and a constraint is placed on the percentage on material used in the space and affects the type of solution that is generated (Bendsöe and Kikuchi 1988).

The "hard-kill' and "soft-kill" methods are also examples of common approaches to topology optimization. Both of these methods focus on removing unnecessary material to generate an optimal topological design. The hard kill option eliminates material much faster than the soft kill method. The hard kill technique removes elements of material experiencing low stress concentrations by replacing the element's elastic modulus with the stress it experiences during each finite element analysis. This means that regions of high stress become harder, while less loaded areas become softer. Thus, the initially homogeneous domain becomes non-homogeneous with varying elastic moduli. This technique however, produces designs that contain stiff material in the load-bearing zones; therefore design solutions may possess regions of considerably large stress concentrations (Mattheck 1997). The soft kill approach weakens or softens the elements by replacing the elastic modulus of each element with its original modulus plus the relative increment of stress it experiences. Specifically, $E_{n+1} = E_n + \Delta\sigma_n$, where, n is the number of finite element analyses and $\Delta\sigma_n = \sigma_n - \sigma_{ref}$. The reference stress, $\sigma_{ref,}$ is defined as the desired component stress. The soft kill option does not remove material as the quickly as the hard kill, but will eventually eliminate the material that is not beneficial to the structure's mechanical properties such as strength and stiffness (Mattheck 1997).

The power law technique is another well-accepted approach to topology optimization. This method is approached by discretizing the design domain into multiple finite elements where the relative density of the material within each element is the design variable. In this technique, the Young's modulus of the material is proportional to the relative density raised to a power. Consider the domain displayed in Figure 2-4, where the grey region represents the design domain with loading and boundary conditions, the black region denotes the solid material, and the white area is to be a void. Using the power law approach to topology optimization, an optimal material distribution for the cantilever beam subjected to a concentrated load (Figure 2-4) can be obtained. The optimal design solution is shown in Figure 2-5 (Sigmund and Tcherniak 2001).

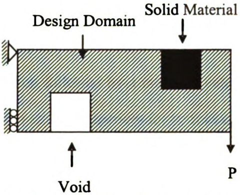

Figure 2-4. Example of topology optimization using the power law approach (Adapted from [Sigmund and Tcherniak 2001])

Figure 2-5. Result from implementation of power law approach (Taken from [Sigmund and Tcherniak 2001])

As previously stated, the optimized structure shown in Figure 2-5 is a design solution produced by the power-law technique, but also resembles a typical design solution that would have been obtained by implementation of the homogenization and hard and soft kill approaches to topology optimization. This design solution (see Figure 2-5) displays an effective distribution of material, however it is geometrically intricate thus difficult and expensive to manufacture. Therefore, alternate techniques must be explored which are capable of optimizing the material distribution within a pre-defined domain, while simultaneously accounting for manufacturing.

In order to account for manufacturing while implementing topology optimization, an alternate technique was investigated. Chellappa et al. proposed a topology optimization technique using a multiresolution method with finite-size features. This approach employs a wavelet-based decomposition (Chellappa et al. 2004) of material distribution followed by a multi-resolution analysis which is then used to generate a library of stiffness matrices for various elements or coupons. Each element can be of different size and, in general, can include more than one perforation. Each coupon is of finite dimension and the effective stiffness matrices of two coupons of different dimensions are typically different. Structures are built and optimized using diverse combinations of the coupons within the library. A typical optimization problem locates optimal patterns of perforations, e.g., to minimize weight (Chellappa et al. 2004). Figure 2-6 displays a typical design solution obtained for a cantilever structure subjected to a concentrated load using the multiresolution approach. The optimized structure has finite features therefore reducing geometric intricacies, thus making it feasible and cost-effective to manufacture.

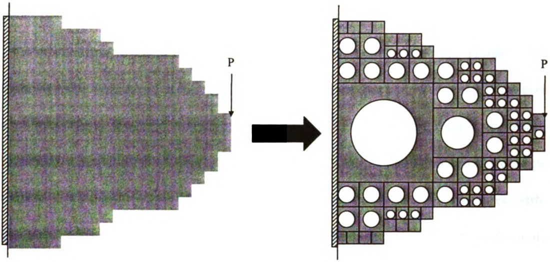

Figure 2-6. Result from implementation of the multiresolution approach (Adapted from [Chellappa et al. 2004])

Given a problem consisting of a defined domain, loading and boundary conditions, and mass and deflection constraints, the most structurally efficient material layout can be determined by implementing topology optimization. Despite the advantages of this technique, most topological algorithms are written to allow for the use of only one objective function, are generally written to define a single loading condition, and do not typically incorporate multiple constraints (e.g. stress and strain). Redefining loading and boundary conditions, integrating constraints, and implementing multiple objective functions would require modifications to the original program or redevelopment of the program in its entirety. Due to this limitation, an alternate optimization procedure was explored to perform material layout optimization for the present work. Without difficult program restructuring, the presented technique permitted the use of multiple objective functions and constraints. This approach is introduced next and presented in detail in Chapter 3.

2.1.3 Parametric Material Layout Optimization

The optimization approach that was implemented for this research was defined to be a material layout optimization technique because it accomplishes goals similar to those intended for shape and topology optimization; although it does not technically fulfill all the criteria associated with either. The optimization technique, which is discussed in more detail in Chapter 3, was conducted on structures with a predefined domain and an initial material layout. The technique was not implemented to optimize the shape of the domain, but the material distribution within the domain using a parametric modeling approach. Specifically, certain parameters were defined prior to optimization and only those parameters were used to control the material layout within the defined boundaries. A specific number of cavities which essentially defined material layout within the structure were established in the initial design. The size and positioning of these theses cavities were capable of changing, however cavities could not be added, removed, or merged. Despite this limitation, the parametric based optimization approach does allow for incorporation multiple objective functions and design constraints and is capable of producing design solutions that account for manufacturing.

2.2 Optimization through Genetic Algorithms

The optimization procedure proposed in Chapter 3 focuses on the use of genetic algorithms (GA's). Genetic algorithms refer to a class of adaptive search procedures using the principle of "survival of the fittest" to locate optimal solutions where the fittest members of an initial population are given better chances of reproducing and transmitting part of their genes to the next generation. (Turkkan 2003, Chou et al.

2001). The method is based on stochastic or random search methods to operate on a population of solutions to locate a global optimum. They are less likely to get "stuck" at local optimums, in comparison to gradient search methods. Genetic algorithms are methods for optimization that work well on combinations of discrete and continuous problem sets. Implementation of a GA requires representation of the solution to a problem as a chromosome. The GA will then create an initial population of solutions and apply a genetic operator such as selection, mutation and/or crossover to evolve into "new" populations of solutions and eventually locate the optimum. Figure 2-7 provides a visual description of the implementation of a genetic operator. Selection, mutation, and crossover operators are applied to the existing population are a population to generate a "new" population of chromosomes. This "new" population is generated by the most "fit" chromosomes from the initially population. A schematic of the GA procedure is shown in Figure 2-8 and presents all the important steps required for proper implemented of a genetic algorithm. These steps will be discussed in greater detail throughout the remainder of Chapter 2.

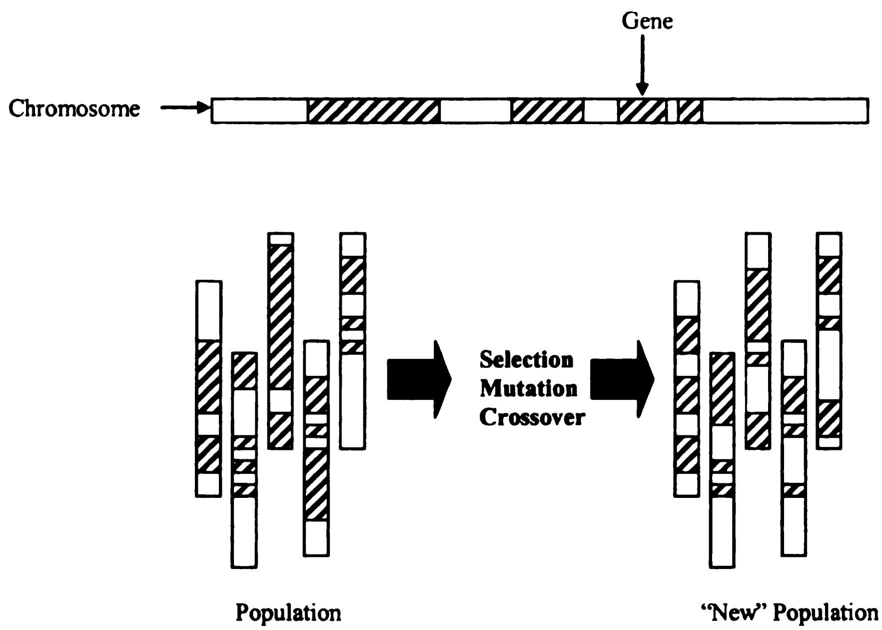

Figure 2-7. Language of genetic algorithms

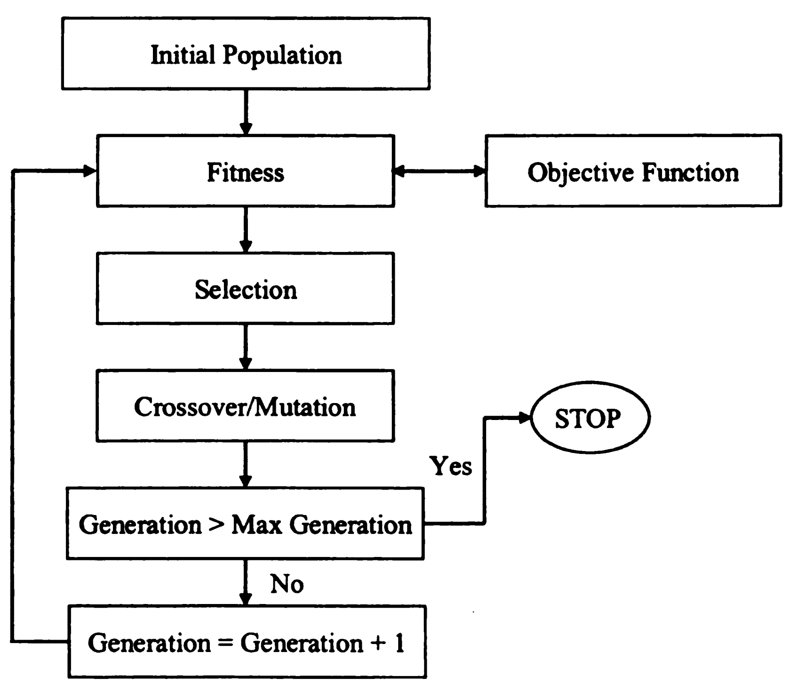

Figure 2-8. Schematic of GA (Adapted from [Turkkan 2003])

Three important aspects must be defined prior to implementing a GA. These include: (1) definition and implementation of the genetic representation, (2) definition and implementation of genetic operators and control parameters, (3) definition of an objective function, and (4) definition of the fitness function (Wall 2001). The following sections will discuss the basic aspects of GA's in more detail.

2.2.1 Definition and Implementation of Genetic Representation

In order to implement a genetic algorithm an appropriate data structure and representation must be defined. The problem characteristics and data structure are usually represented in the format of a chromosome string. The data structure should include all relevant parameters of the problem and uniformly symbolize all possible solutions. For example, if the function being optimized is of real numbers, real numbers should be chosen in the chromosome. On the other hand, if imaginary numbers and integer values are observed in the objective function, the chromosome should be defined with those characteristics. The chosen representation must be able to represent all solutions to the problem, but if possible, representation of infeasible solutions should be eliminated. If the chromosome is capable of representing infeasible solutions, the objective function must be designed to give them partial credit, so that they do not reproduce and/or exist in multiple future generations. The representation should not contain information beyond what is necessary to represent a solution to the problem since this tends to increase the size of the search space and impede the performance of the GA (Wall 2001). For examples, if the problem depends on a sequence of items, an order-based representation can be selected. If this is the case, the genetic operators must be chosen so that the reliability of the sequence is maintained. Common structures used for representation include a list, an array, or a tree structure (Figure 2-9) (Wall 2001).

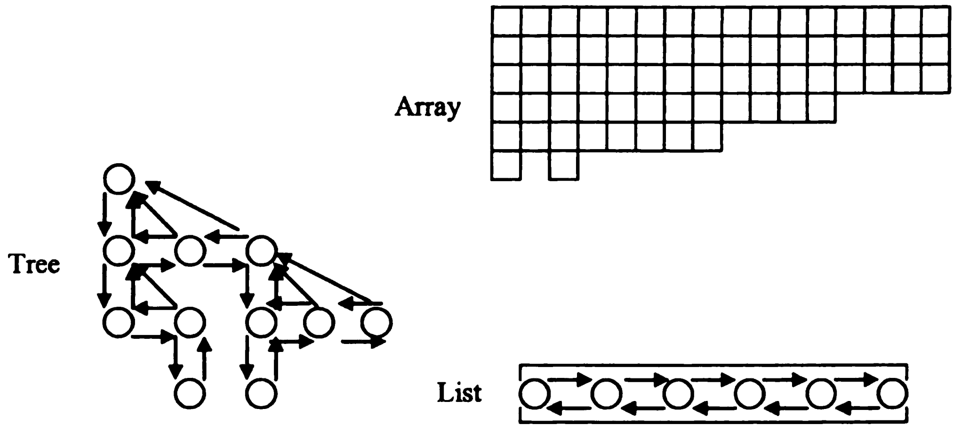

Figure 2-9. Possible structures used for representation of individual chromosomes (Adapted from [Daves 1991]).

Some problems include a combination of continuous and discrete variables. In this case, it may be necessary to create a new structure to store the mix of information and the genetic operators must be defined so that the structure of the solution is not affected. Specifically, a solution containing integer values and real numbers might use a crossover operator that crosses the integer values with one another and the real numbers with one another, but does not mix the two values. Ultimately, the genetic operators must be chosen so that they are appropriate for whichever representation is selected (Wall 2001).

2.2.2 Definition and Implementation of Genetic Operators and Control Parameters

Genetic operators are used in genetic algorithms to generate diversity and to combine existing solutions with others (Guervos 1997). Three primary genetic operators can act upon a chromosome and include: selection, mutation, and crossover. Using these operators, an initial population can be favored, a mutation or crossover corresponding to the genetic representation can be defined, and alterations of the genetic algorithm can be made as the population evolves (Wall 2001).

2.2.2.1 The Selection Operator

The selection operator gives preference to the better, or more "fit," designs, or individuals, allowing them to pass their "genes" onto the next generation. Researchers recommend using an enlarged sampling approach for the selection process, which is used to reduce the amount of duplicating chromosomes entering a population during selection. Two enlarged sampling approaches exist, the $(\mu + \lambda)$ and the (μ, λ), where μ is the number of parents and λ is the number of offspring. The "comma" or "plus" determines the type of selection process used in choosing the new parental generation (Beyer 2000, Chou et al. 2001, Lagaros 2002).

The "comma" selection method is a process of competing offspring. It begins when μ parents produce λ children through mutation. The μ parents are discarded, leaving only the children to compete directly with one another. The children are then assigned a fitness value based on their quality considering the problem specific conditions that they are in. The best individuals of the λ children are selected as the next parental generation. This technique is capable of diverging due to the fact each parent can only produce children once in the entire process, resulting in possible elimination of the most-fit individuals (Lagaros 2002, Beyer 2000).

The "plus" selection method involves competing parents and offspring. This process is implemented when μ parents produce λ children by mutation. Each child is then assigned a fitness value and the best or fittest individuals of both the parents and offspring become the next generation's parents. This selection process has proven to be more effective due to fact that both parents and children can survive through multiple generations. The more elite or fit will remain, and the weak are eliminated, therefore possible solutions will not be discarded throughout the process (Lagaros 2002).

2.2.2.2 The Mutation Operator

The mutation operator plays two important roles in GA's: (1) it provides and maintains diversity within a population to prevent premature convergence and (2) it can work as a search operator. The mutation operator makes alterations to an individual chromosome rather than combining parts of two or more chromosomes as is done with the crossover technique. Mutation can alter a single field, multiple fields, or all fields of an existing chromosome. For example, if a child has a given chromosome structure consisting of five 2-bit fields, the single, multiple, and all-field mutation would be as shown in Figure 2-10. (Daves 1991, Goodman 2002).

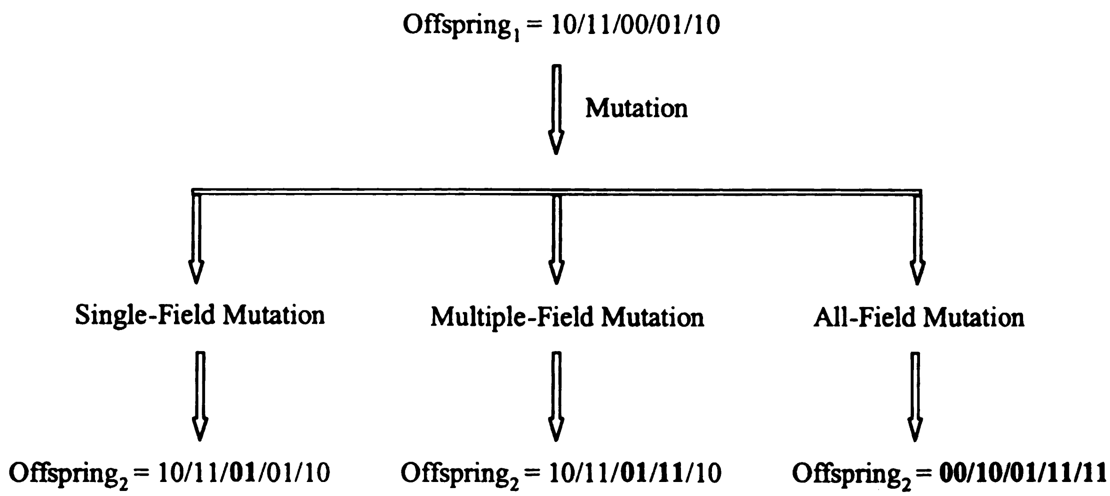

Figure 2-10. Examples of mutation

2.2.2.3 The Crossover Operator

Like the mutation operator, the crossover operator also allows for exploration of a new solution space. Three main types of crossover methods exist in GA's and include: one point, two point, and uniform crossover. In one-point crossover, a random position along a pair of chromosomes is generated. The bits from a fixed position on the first chromosome to the end are swapped with the second chromosome in the same range. In the process, the bits from the second chromosome are transferred to the corresponding bits in the first chromosome. For example, if parent 1 and parent 2 have the following chromosome structure (Chou et al. 2001):

$\text{Parent}_1 = 101010 \vdots 10101$

$\text{Parent}_2 = 111001 \vdots 00111$

Crossover Point

The generated offspring would be:

$\text{Offspring}_1 = 101010 \vdots 00111$

$\text{Offspring}_2 = 111001 \vdots 10101$

Crossover Point

Two-point crossover is an enhancement of one-point crossover approach and is designed to explore a wider search space. With this method, the chromosomes are thought of as rings with the first and last gene connected. The rings are cut in two positions and the resulting portions are swapped. For example, if parent 1 and parent 2 have the following chromosome structure (Chou et al. 2001):

$\text{Parent}_1 = 10 \vdots 1010 \vdots 00111$

$\text{Parent}_2 = 11 \vdots 1001 \vdots 10101$

Crossover Points

The generated offspring would be:

$$Offspring_1 = 11\ 1010\ 10101$$

$$Offspring_2 = 10\ 1001\ 00111$$

Crossover Points

Uniform crossover is a process which involves random selection of bits to form offspring. This crossover technique results in only one offspring, as opposed to the two produced by the one and two-point crossover methods. Specifically, each bit of the offspring is randomly chosen from the corresponding bits of the parents. For example, if parent 1 and parent 2 have the following chromosome structure (Chou et al. 2001):

$$Parent_1 = 11101010101$$

$$Parent_2 = 10100100111$$

The generated offspring could be:

$$Offspring_1 = 11100000111$$

2.2.2.4 Control Parameters

Various control parameters can be used to vary a genetic algorithm. These parameters include: (1) crossover rate, (2) mutation rate, (3) generation gap, (4) population size, (5) scaling and (6) stopping criteria. The crossover rate defines the probability of crossover occurring between two chromosomes. Mutation rate is the probability that a value in a chromosome will be changed. The generation gap identifies the proportion of the population that will be replaced with new offspring.

The scaling parameter controls the fitness function to magnify the differences between chromosomes. This magnification assists in maintaining competition in the search space to prevent premature convergence which may be based on a few highly fit chromosomes. The stopping criteria are directly related to termination of the evolution process. This could be based on a number of cycles, fitness convergence, or other criteria (Chou et al. 2001).

2.2.3 The Objective Function

The objective function, also known as the goal function, is the function to be optimized and is used to determine how "good" or "fit" each individual is. This process involves the evaluation of the individuals and determination of a fitness value. After a fitness value is determined, the selection process is then implemented again and the best individuals from the present generation are selected for the new generation. The fitness of each individual is defined by a value, which reflects how well an individual solves the task at hand. This value, along with generational age is used to determine the number of times any individual is replicated (see Section 2.2.4) (Daves 1991).

2.2.4 The Fitness Function

The "fitness function" quantifies the optimality of a solution in a genetic algorithm such that a particular design may be ranked against all other designs. This function is generated on the basis of the objective values of the individual in comparison with all other individuals in the selection pool. The fitness function is used to map a chromosome to a fitness value and may be dependent on the objective function, different constraints and/or stochastic influences. The best fit individuals are those who will survive in their existing environments and whose descendents will most likely adapt or thrive in future environments (Daves 1991).

3 DEVELOPMENT AND IMPLEMENTATION OF PARAMETRIC MATERIAL LAYOUT OPTIMIZATION TECHNIQUE

3.1 Overview

This chapter presents the development and implementation of a parametric approach to material layout optimization. This computational study was completed through implementation of the following objectives: (1) development of the optimization procedure, (2) validation of the proposed optimization technique, and (3) application of this technique to a specific case study. These three tasks are introduced and discussed in detail throughout the remainder of this chapter.

3.2 Overview of the Optimization Technique

The optimization technique presented in this thesis focuses on an idea similar to that of topology optimization, which is to distribute material efficiently throughout a defined structural domain subject to loading and boundary conditions. Topology optimization techniques make possible the identification of optimal solutions to material distribution; however these solutions (i.e. optimal designs) may be rather extensive with detailed geometries that may create difficulties in manufacturing biocomposite components due to their random nature and fluffy, cotton-like texture (Chapter 1). This limitation has been addressed through recent efforts that propose methods resulting in design solutions with simple domain geometries. One example used to generate simplified geometries is through implementation of the multiresolution technique (Chellappa et al. 2004) (Chapter 2), which involves the formulation of a finite element code that pre-defines the boundaries of the structure and only allows the material distribution within the domain to change. The limitation of the multiresolution technique, however, is that in order to incorporate of multiple objective functions and constraints, re-formulation of the finite element program is necessary. To avoid this limitation, it is also possible to approach the problem by using existing finite element programs together with parametric modeling. In this method, simultaneous implementation of finite element software and a general purpose optimization program allow the optimal material distribution within a defined structural domain for maximum stiffness to be obtained.

The global optimization problem studied for this thesis was approached using parametric modeling and finite element analyses conducted with the commercial program ABAQUS (Hibbitt et al. 2004) and solved using a genetic algorithm implemented through the commercial software package, HEEDS (Red Cedar Technology 2004). HEEDS is a general purpose optimization software package that automates the search for optimal solutions within a given design space through the use of different mathematical optimization algorithms (gradient-based, genetic algorithms, simulated annealing, design of experiments, etc.). The development of the optimization procedure was initiated by modeling and analyzing an initial design in ABAQUS CAE, ABAQUS pre-processor, by means of a script file that defined geometric parameters within the domain, i.e. void size, positioning, etc. HEEDS altered the defined parameters within the existing base design by means of the ABAQUS CAE script file to create a modified or "new" script file. A finite element analysis was then conducted with ABAQUS to evaluate the "new" design. The fitness function of each design was then assessed using HEEDS according to the optimization problem formulation. The process is iterative and was repeated until design time was exhausted (Figure 3-1). Exhausting the design time was the stopping criteria of the particular GA implemented by HEEDS and was dependent on the number of cycles defined by the user. Even though this criterion was not based on fitness convergence, it was still capable of being detected. For example, if the comparison in the fitness value of the last few designs was within a small percentage of one another, convergence can be assumed. Furthermore, convergence can be assumed if the last design saved was obtained approximately 10 cycles prior to completion of the last cycle.

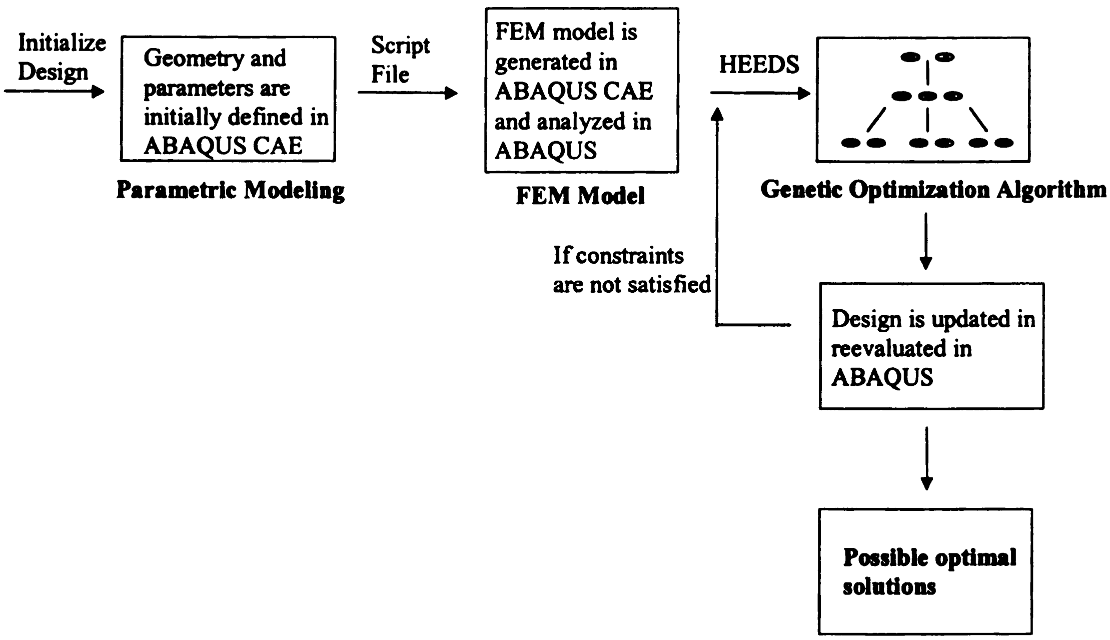

Figure 3-1. Optimization flowchart

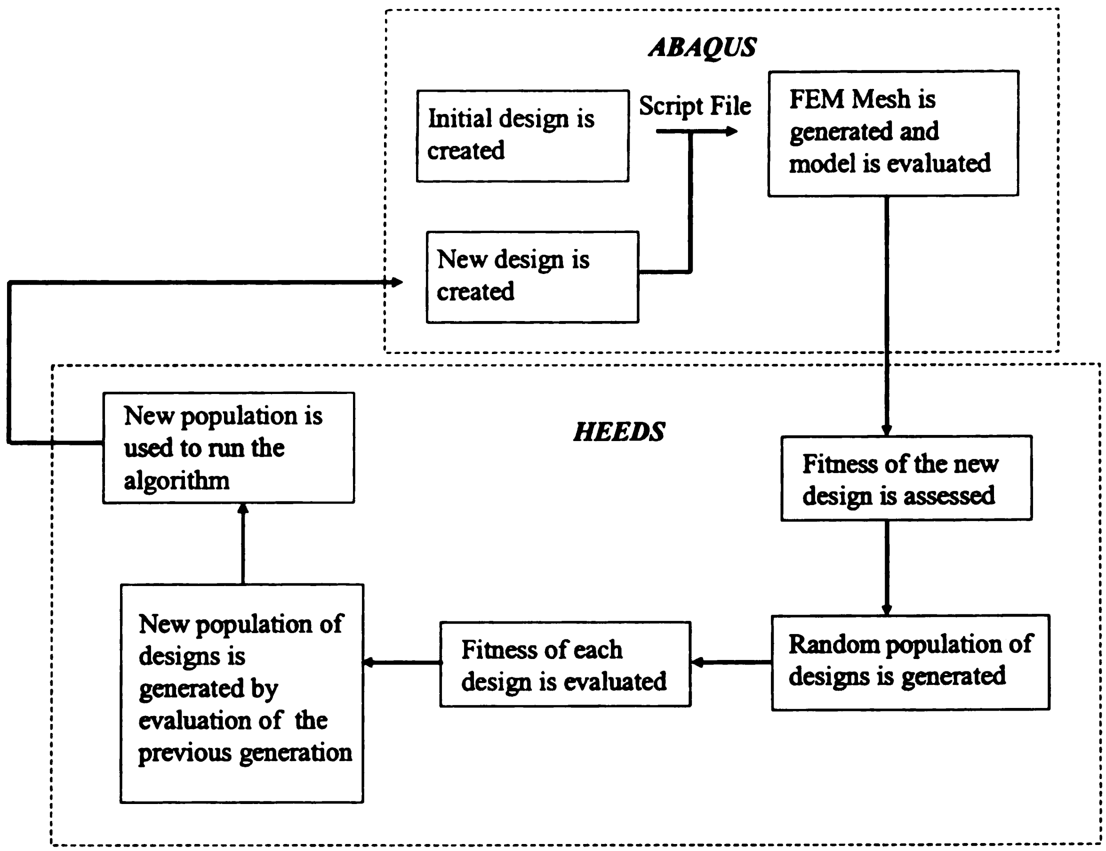

Figure 3-2. Optimization process

The optimization process starts with HEEDS randomly selecting values for specified design variables within user-defined limitations (i.e. variable bounds). The design variables are defined as the geometric parameters i.e. void size, positioning, etc. within the initial ABAQUS CAE script file and are altered by HEEDS to control the re-modeling of each existing design to create a new one. The ABAQUS CAE generated script file, typically referred to as the python file, (model.py), which is modified by HEEDS, is then fed back into ABAQUS for re-meshing and analysis. This process is repeated with ABAQUS CAE creating multiple re-modeled designs and the fitness (fitness formulation will be discussed in later section) of each being evaluated by HEEDS (i.e. analyses were performed). The first design is saved to the

HEEDS working files as the benchmark design and new designs are added when a better design is found. HEEDS continues to alter the design variables within the ABAQUS CAE script file to generate new designs until the number of cycles has completed. The optimization process described above (Figure 3-1 and Figure 3-2) is schematically shown in Figure 3-3.

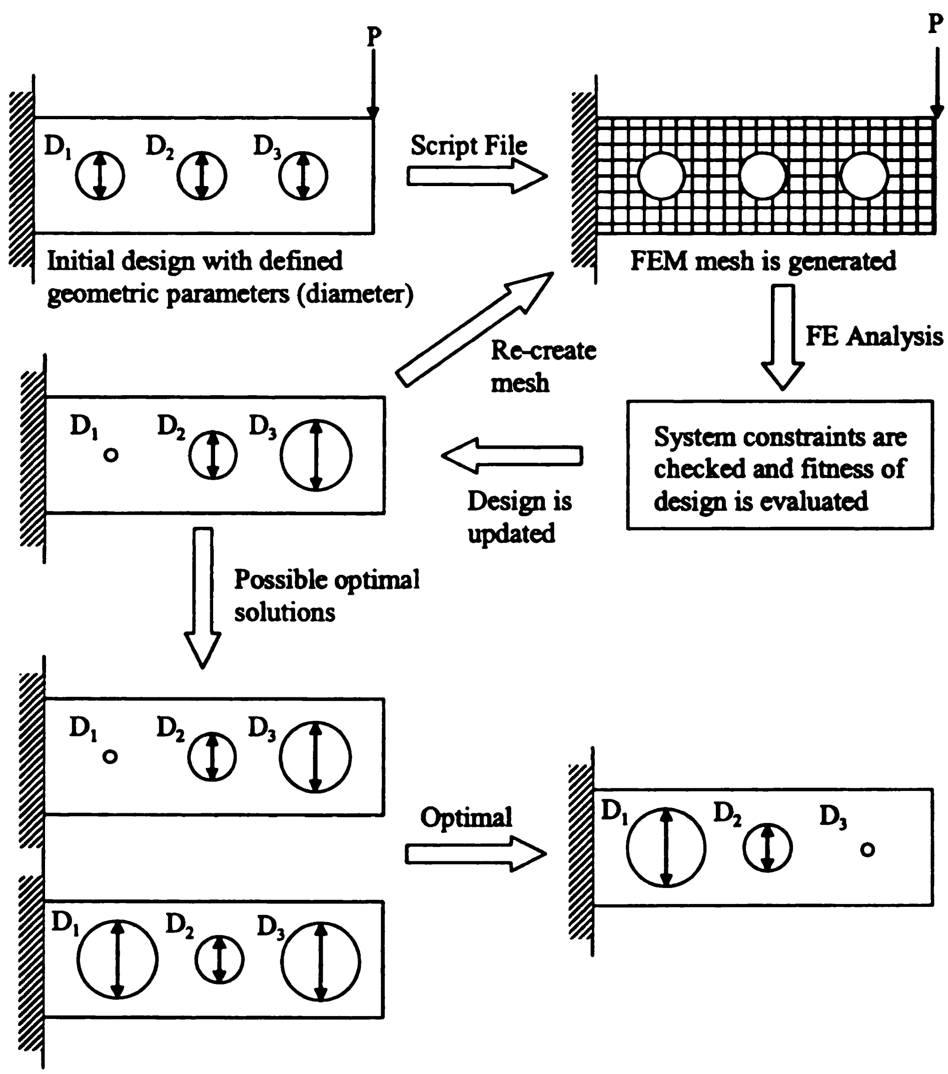

Figure 3-3. Schematic of optimization procedure

3.3 Validation of the Optimization Procedure

The proposed optimization procedure was validated by comparing its performance in solving standard topology optimization problems against those obtained with well-accepted topology optimization methods. Thus, the optimal solutions obtained through the parametric approach were compared to "known" solutions generated by employing actual topology optimization techniques. If the results were similar, the proposed optimization method was considered valid for the overall goal of obtaining an optimized material layout. The validation procedure included six major tasks: (1) problem definition, (2) parametric modeling, (3) optimization problem formulation, (4) implementation of the optimization process, (5) evaluation of optimal solutions, and (6) validation of optimal solutions. These tasks are discussed in detail in the following sections.

3.3.1 Problem Definition

Validation of the proposed parametric optimization procedure was conducted through the optimization of two classical topology problems: The standard problems were borrowed from literature and include: (1) the Messerschmitt-Bölkow-Blohm Beam (MBB-beam) (Olhoff et al. 2004) and (2) the 8-bar truss (Rozyany et al. 1992). These problems have been used extensively by researchers to evaluate topology optimization algorithms. The MBB-beam is a simply supported beam with an aspect ratio of 1/5 (Figure 3-4) and the 8-bar truss is a short cantilevered beam with an aspect ratio of 5/8 (Figure 3-5). Both problems are defined as having concentrated unit loads and with a unit Young's modulus.

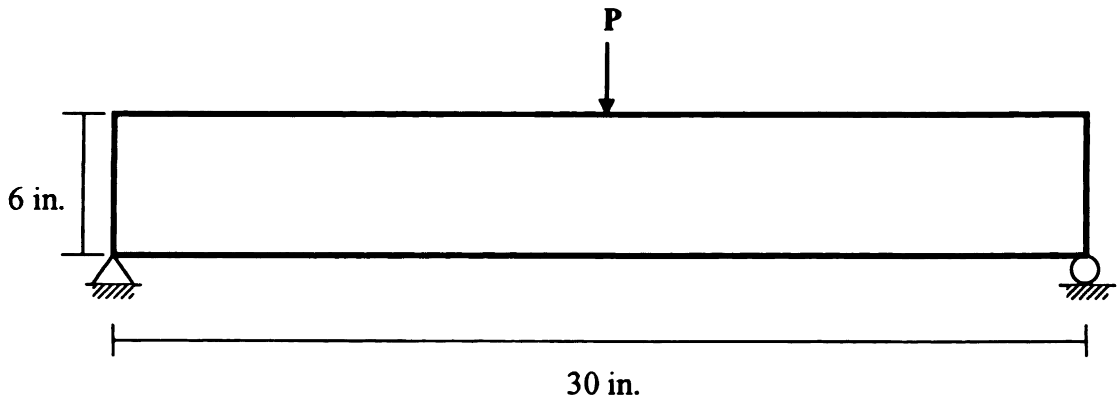

Figure 3-4. MBB-beam

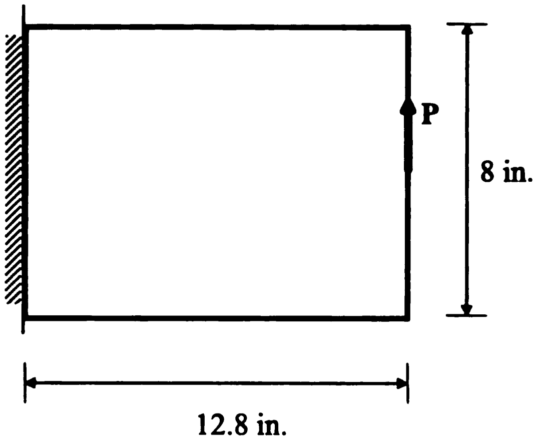

Figure 3-5. 8-bar truss

3.3.2 Parametric Modeling

Since the goal was to optimize the structural or material arrangement within the pre-defined domain, the parametric model must allow for redistribution of material. To accomplish this, an initial design with a pre-defined layout was created for both the MBB-beam and the 8-bar truss (see Figure 3-6 and Figure 3-7) and the radii of each void were identified as the parameters to control the design features or material layout. The parameters (i.e., the radii of each void) were identified through ABAQUS CAE by means of a script file that was then linked to the optimizer. The optimizer uses this ABAQUS script file to read the parameters (i.e radii) and randomly alter them to generate a modified script file. This modified script file is then used by ABAQUS to create a parametrically remodeled design. This parametric remodeling occurs throughout each of the design iterations prior to re-meshing and FE analysis.

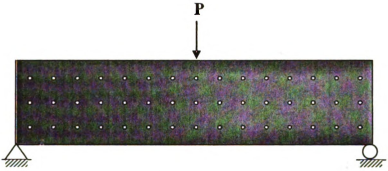

Figure 3-6. Parametric model for MBB-beam (intial design)

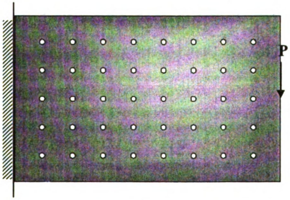

Figure 3-7. Parametric model for 8-bar truss (initial design)

Changes to the parameter values (radii) throughout the optimization process are controlled by the definition of design variables within the optimization problem formulation. Details of the problem formulation are discussed in the following section.

3.3.3 Optimization Problem Formulation

The optimization problem formulation includes identifying and defining the optimization algorithm, genetic operators and control parameters, and formulation elements such as design variables, system constraints, objective function, and the fitness function for the both the MBB-beam and the 8-bar truss.

The algorithm chosen within HEEDS capabilities for the presented parametric layout optimization approach was a general genetic algorithm. Genetic algorithms use a stochastic or random search method to create a population of designs. Design variables, which define the design solution, are typically represented in binary form as a continuous string resembling a chromosome. Through the implementation of crossover and mutation operators, individuals in the current population evolve into new populations of individuals and the fitness of each chromosome is evaluated. The process continues until the total number of user defined cycles is completed (Chapter 2) (Wall 2001).

The genetic operators chosen for the optimization procedure were multi-field mutation (Chapter 2) and one point crossover (Chapter 2). Multi-field mutation allowed for alteration in multiple fields within each chromosome (Goodman 2002). The one-point crossover operator selects a common, random crossover point in two parents and then swaps the corresponding bits to generate offspring (Daves 1991)

The control parameters defined for the general genetic optimization technique include: (1) mutation rate, (2) crossover rate, (3) population size and (4) stopping criteria. For the presented parametric optimization technique, the mutation rate was defined to be 20%, which means that the values in each chromosome would have a 20% probability of changing. Similarly, the crossover rate was defined to be 50% (i.e. a 50% crossover probability between chromosomes). Lastly, the population size was set equal to 60. Choosing a larger population size increases the number of evaluations performed per cycle, enhancing diversity within each design and, most importantly, assisting in preventing premature convergence. The stopping criterion for this genetic algorithm was dependent on the number of cycles, which was set to a value of 75. Once the 75 cycles was completed the optimization problem was terminated. Even though this stopping criterion is not based on fitness convergence, it is capable of being detected. For example, if the comparison in the fitness value of the last few designs is relatively close in value, convergence can be assumed. Furthermore, convergence can also be assumed if the last design saved was obtained approximately 10 cycles prior to the completion of the last cycle. A summary of the genetic operators and control parameters is shown in Table 3-1.

Table 3-1. Summary of genetic operators and control parameters

Genetic Operators
Multi-field Mutation
One-Point Crossover

Control Parameters

Mutation Rate	Crossover Rate	Population Size	Stopping Criterion
20%	50%	60	75 Cycles

Design variables are used to model the specific parameters that influence the system performance. Variables can be represented as continuous or discrete sets, and/or as dependent variables. Optimization for the MBB-beam and 8-bar truss was performed twice, once using continuous variable sets and once using discrete variable sets the radii to account for manufacturing. In both attempts at optimization, dependent variables were also defined. The design variables were used to represent the radii of each void in the initial design layout (Figure 3-6 and Figure 3-7). The continuous and discrete sets were formed by defining virtual regions around each void and restraining them to increase or decrease in diameter within that region. The surrounding areas encompassing each void were 2 in. × 2 in. for the MBB-beam, resulting in 45 virtual square elements (Figure 3-8); and 1.6 in. × 1.6 in. for the 8-bar truss, resulting in 40 elements (Figure 3-9). Each void was numbered so that a corresponding radius could be defined. For example, the voids in the upper left hand corners of Figure 3-8 and Figure 3-9 were assigned a corresponding radius of r_1, and continued along the rows, completing with the voids in the lower right hand corners which were identified as having a radius of r_{45} and r_{40}, respectively

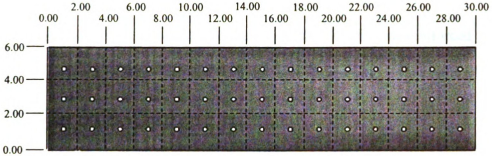

Figure 3-8. Virtual square elements within the domain of the MBB-beam (dimensions shown in inches)

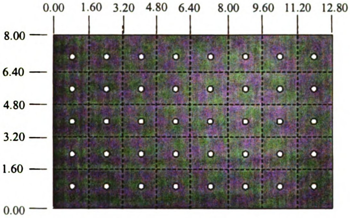

Figure 3-9. Virtual square elements within the domain of the 8-bar truss (dimensions shown in inches)

The continuous and discrete variable sets used in both attempts at optimization of the MBB-beam and 8-bar truss problems were defined such that each void in the base design was allowed to increase to a maximum of 90% of its surrounding virtual region, thus preventing void overlap and exceeding of the domain. The continuous variable set was defined such that the radius of each void could range in value from 0.05 in. to 0.9 in. with increments of 0.01 in., while the discrete variable set was defined using a set of 4 values: 0.05 in., 0.25 in. 0.55 in., and

0.9 in. Some of the variables were defined as dependent due to the symmetric response present in both systems. Thus, a symmetry condition was enforced along a vertical plane for the MBB-beam (see Figure 3-10) and along a horizontal plane for the 8-bar truss (see Figure 3-11).

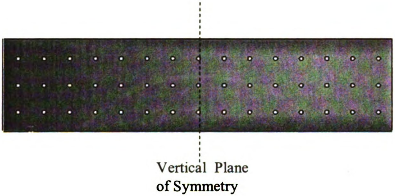

Figure 3-10. Plane of symmetry enforced on MBB-beam

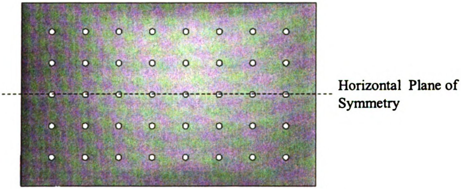

Figure 3-11. Plane of symmetry enforced on 8-bar truss

Constraints represent the limitations or specifications that a variable is subjected to and are used to guide the optimization process since optimal solutions are searched only amongst those that satisfy them (Arora 1989). The optimization problems for the MBB-beam and the 8-bar truss were formulated using a single system constraint. A mass constraint governed the design and was defined by implementing a relative density (Equation 3.1) of 0.65 for the MBB-beam and 0.70 for the 8-bar truss which were values borrowed from literature (Chellappa et al. 2004). Specifically, the mass of the optimized MBB structure was constrained to be no more than 65% of the mass of an identical structure with zero voids. Similarly, the mass of the optimized 8-bar truss was unable to exceed 70% of the mass of an identical structure with zero voids.

$$\frac{M_{optimizeddesign}}{M_{solid}} = \rho_{relative} \tag{3.1}$$

The objective function is the optimized target that minimizes or maximizes a specific aspect of the model (Daves 1991). The objective function for the MBB-beam and 8-bar truss optimization problems was to minimize strain energy. This objective was chosen since the goal is to obtain the stiffest structure possible with a given amount of material. Clearly, strain energy and mass are indirectly related, since as material is removed the mass reduces, which increases the strain energy. Table 3-2 through Table 3-5 summarize the formulation of the optimization problems implemented for the two validation models. These formulations were defined in the HEEDS optimizer prior to process initiation.

Table 3-2. Optimization problem formulation for MBB-beam

Find:	r_n, where n = void number = 1-8, 16-23, 31-38 (integers)
That minimizes:	Strain Energy
Subject to:	Mass constraint

Find:	r_n, where n = void number 1-8, 16-23, 31-38 (integers)
That minimizes	$f(x) = \int_V \sigma\varepsilon \, dv$
Subject to:	$g_i(x) \leq 0$, i = 1- n constraints

Table 3-3. Summary of formulation elements for the MBB-beam

Formulation Elements	Variable Type	Definition of Formulation Element	
Design Variables	Discrete/Continuous	Void Radii	r_n, where n = void number = 1-8, 16-23, 31-38 (integers)
	Dependent	Void Radii	r_n, where n = void number = 9-15, 24-30, 39-45 (integers)
	Parameter	Length	12.8 in.
	Parameter	Height	8 in.
Constraints		Mass	$M \leq 117$ lbs
Objective Function		Minimize Strain Energy	

Table 3-4. Optimization problem formulation for the 8-bar truss

Find:	r_n, where n = void number = 1-24 (integers)
That minimizes:	Strain Energy
Subject to:	Mass constraint

Find:	r_n, where n = void number = 1-24 (integers)
That minimizes	$f(x) = \int_V \sigma\varepsilon \, dv$
Subject to:	$g_i(x) \leq 0$, i = 1- n constraints

Table 3-5. Summary of formulation elements for the 8-bar truss

Formulation Elements	Variable Type	Definition of Formulation Element	
Design Variables	Discrete/Continuous	Void Radii	r_n, where n = void number = 1-24 (integers)
	Dependent	Void Radii	r_n, where n = void number = 25-40 (integers)
	Parameter	Length	12.8 in.
	Parameter	Height	8 in.
Constraints		Mass	$M \leq 71.68$ lbs
Objective Function		Minimize Strain Energy	

As stated in Chapter 2, the fitness function is used to determine the optimality of a solution in a genetic algorithm and may be dependent on different constraints and/or stochastic influences. The fitness function defined in the optimizer, HEEDS, for a genetic algorithm is dependent on the objective function and design constraints. The fitness value is obtained as follows (see Equation 3.2):

$$\text{Fitness Value} = \text{Objective Function} - (\text{Penalty Function} * \text{Constraint Violation})$$

Specifically, for optimization of the two validation problems:

$$f = \frac{E}{NormalizingCoefficient} - [10{,}000 * (M_{allowable} - M_{violated})] \quad (3.2)$$

where, E is the strain energy and M is the mass.

This function is evaluated by HEEDS at the end of each design iteration and the fitness level of the design is dependent the obtained value. The most "fit" design (i.e, the design with the highest fitness value) when the number of user defined cycles has exhausted is considered the best design. It is only considered optimal if the fitness value of the prior designs was similar to that of the last design obtained or the last design obtained was found approximately 10 cycles prior to completion of the last cycle.

3.3.4 Implementation of Optimization Process

In order to implement the optimization procedure, it was necessary to link the parametric model to the problem formulation, which was done within the HEEDS optimizer. The connection was performed by means of the script file that is generated after creation of the initial design through ABAQUS pre-processor: ABAQUS CAE. The task of the optimizer was to randomly select values for the design variables, or controlling parameters, within the defined continuous and discrete variable sets (see Section 3.3.2) to alter the parameters in the existing ABAQUS script file. The modified script file was then used by ABAQUS CAE, to generate and re-mesh a new model. The parametrically remodeled design could then be analyzed by ABAQUS which would retrieve the output values needed to evaluate the fitness in HEEDS. Through continuous alteration of the design variables/controlling-parameters a collection of new designs could be created. The optimizer saves the first design as a benchmark design and a new design is added when a better one is found. The process is repeated until the number of user defined cycles has been reached. The last design saved by the optimizer can be considered optimal if its fitness value compares favorably to the two or three prior designs that were saved or if the last design saved was obtained approximately 10 cycles before the maximum amount of cycles was reached.

3.3.5 Evaluation of Optimal Solutions

Using the optimization problem formulations displayed in Table 3-2 through Table 3-5 in the previous section, the proposed procedure was implemented using both the continuous and discrete variable sets to optimize the material layout of the MBB-beam and the 8-bar truss problems. It was found that the difference in results when using the continuous variable sets and discrete variable sets were minimal; with optimization using the discrete variable sets producing design solutions for both the MBB-beam and the 8-bar truss problems that were more comparable to those obtained through the well-established topology optimization techniques (Section 3.3.6). Therefore, the design solutions and evaluation history displayed in this section only represent those obtained through optimization with the discrete variable sets.

The parametric modeling approach to optimization produced multiple designs for both problems throughout the multiple cycle run time. In the early stages of optimization various designs were produced, but a steady and immediate decrease in strain energy was not apparent (Figure 3-12 and Figure 3-13). However, as the procedure advanced the designs seemed to evolve from one another and progressively improved (see Table 3-6 and 3-7). The relative densities of each structure began to approach the maximum allowable value and the strain energy continued to decrease. The design solutions obtained were those with the lowest strain energy and with relative densities of 0.65 for the MBB-beam and 0.70 for the 8-bar truss (Figure 3-14 and Figure 3-15). These solutions could be considered optimal since they were saved by HEEDS approximately 10 cycles prior to completing the allowed number of 75 cycles. Thus, no improved designs were found for several cycles before concluding the optimized search.

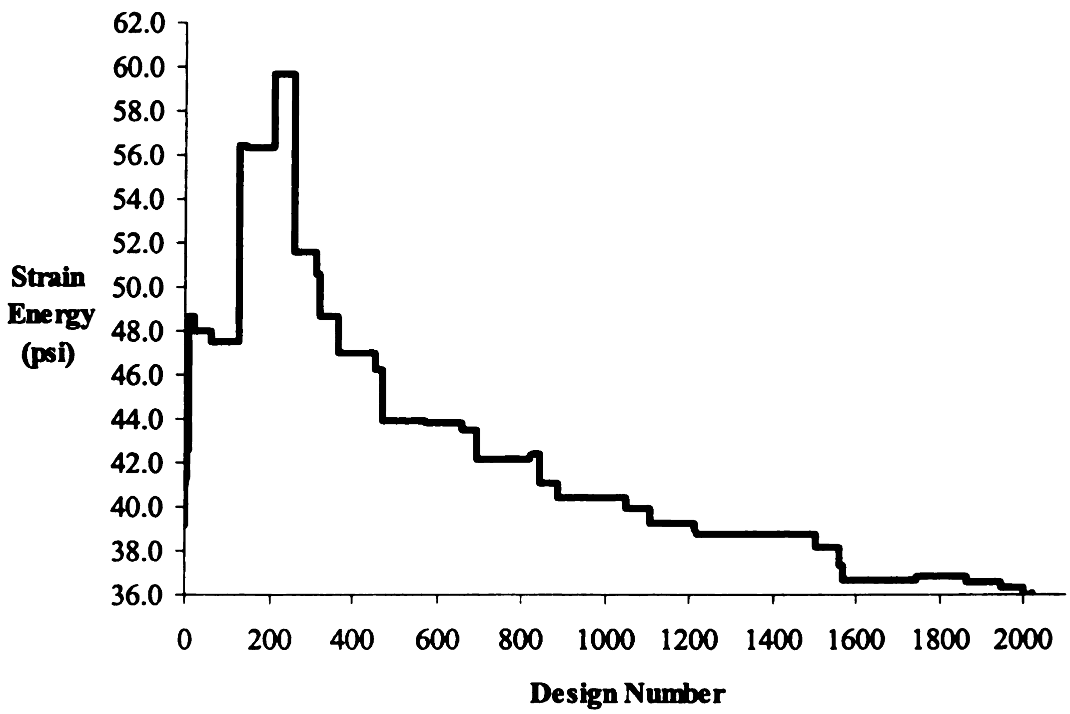

Figure 3-12. Optimization history of MBB-beam problem using a discrete variable set

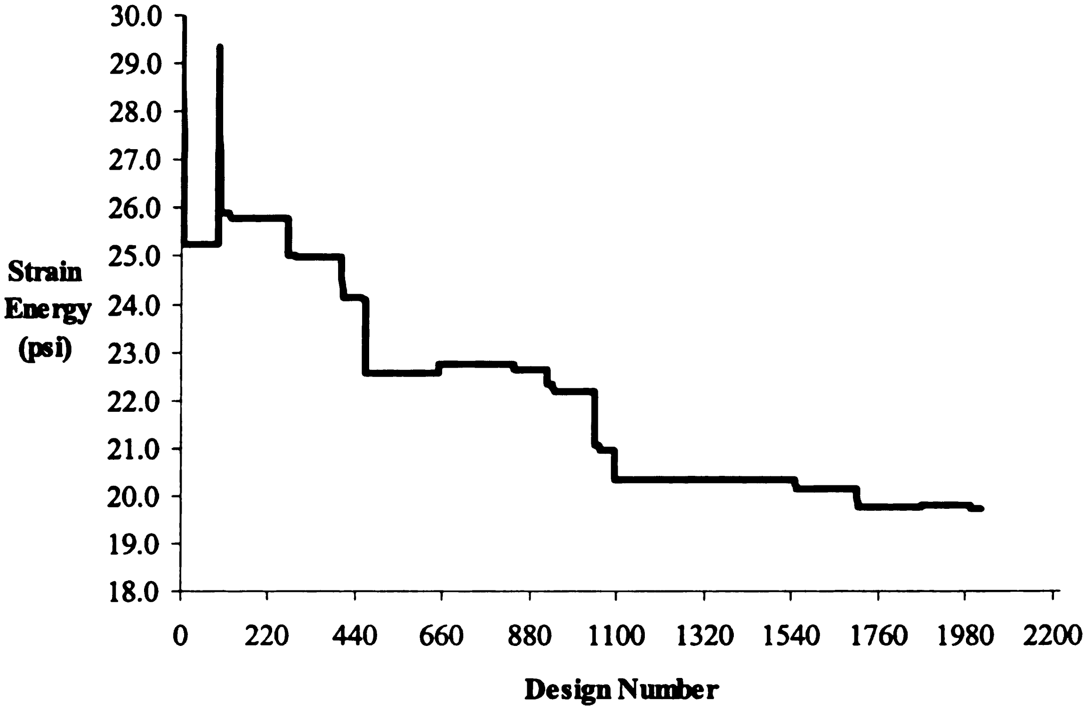

Figure 3-13. Optimization history of 8-bar truss problem using a discrete variable set

Table 3-6. Evolution of designs for the MBB-beam problem

Design	Design Number	Mass (lbs)	Strain Energy (psi)	Relative Density
	1	137.13	3.92E+01	0.762
	3	129.74	4.26E+01	0.721
	10	126.38	4.87E+01	0.702
	24	125.00	4.80E+01	0.694
	61	124.87	4.75E+01	0.694
	128	120.83	5.64E+01	0.671
	146	120.24	5.63E+01	0.668
	211	111.24	5.97E+01	0.618
	259	115.18	5.16E+01	0.640
	312	116.45	5.06E+01	0.647
	322	116.64	4.87E+01	0.648
	365	114.95	4.70E+01	0.639
	454	117.27	4.62E+01	0.652
	472	117.14	4.39E+01	0.651
	570	117.05	4.38E+01	0.650
	658	116.83	4.35E+01	0.649
	694	117.69	4.22E+01	0.654
	824	117.22	4.24E+01	0.651
	843	116.62	4.11E+01	0.648
	889	116.34	4.04E+01	0.646
	1052	117.23	3.99E+01	0.651
	1107	116.10	3.92E+01	0.645

Table 3-3. Evolution of designs for the MBB-beam problem (cont.)

Design	Design Number	Mass (lbs)	Strain Energy (psi)	Relative Density
	1215	117.11	3.88E+01	0.651
	1502	115.87	3.81E+01	0.644
	1528	117.00	3.81E+01	0.650
	1560	117.58	3.73E+01	0.653
	1569	117.62	3.66E+01	0.653
	1743	117.48	3.68E+01	0.653
	1864	117.14	3.66E+01	0.651
	1946	117.42	3.63E+01	0.652
	1998	117.36	3.60E+01	0.652
	2019	117.04	3.61E+01	0.650

Table 3-7. Evolution of designs for the 8-bar truss problem

Design	Design Number	Mass (lbs)	Strain Energy (psi)	Relative Density
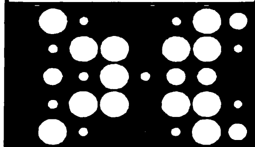	1	73.90	3.18E+01	0.722
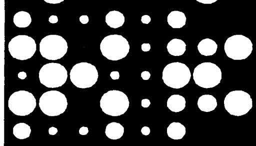	3	71.72	2.52E+01	0.700
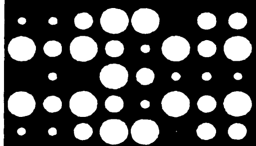	94	67.9	2.94E+01	0.663
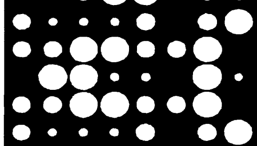	96	70.77	2.59E+01	0.691
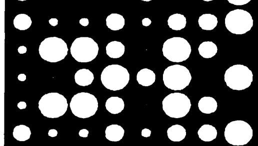	123	70.76	2.58E+01	0.691
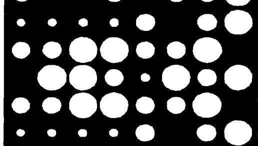	269	69.05	2.50E+01	0.674
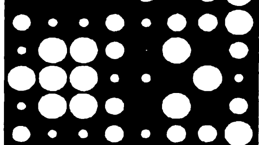	289	70.18	2.50E+01	0.685
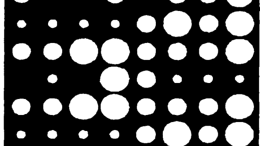	406	69.46	2.41E+01	0.678
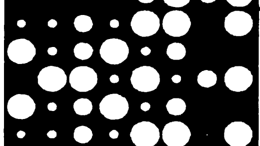	457	70.32	2.41E+01	0.687
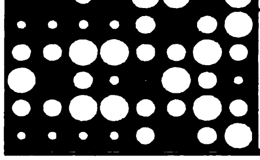	464	70.81	2.26E+01	0.692

Table 3-4. Evolution of designs for the 8-bar truss problem (cont.)

Design	Design Number	Mass (lbs)	Strain Energy (psi)	Relative Density
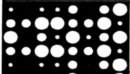	648	70.58	2.28E+01	0.689
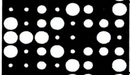	794	69.81	2.28E+01	0.682
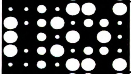	840	70.18	2.27E+01	0.685
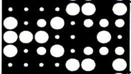	924	69.02	2.23E+01	0.674
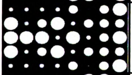	939	70.59	2.22E+01	0.689
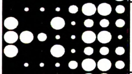	1045	70.96	2.11E+01	0.693
	1052	70.78	2.10E+01	0.691
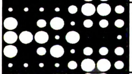	1058	69.96	2.10E+01	0.683
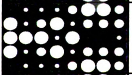	1096	69.99	2.03E+01	0.683
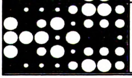	1551	70.33	2.02E+01	0.687

Table 3-4. Evolution of designs for the 8-bar truss problem (cont.)

Design	Design Number	Mass (lbs)	Strain Energy (psi)	Relative Density
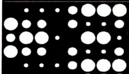	1708	70.72	1.98E+01	0.691
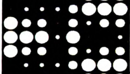	1870	70.36	1.98E+01	0.687
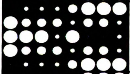	1994	70.03	1.97E+01	0.684
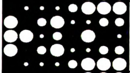	2071	70.50	1.95E+01	0.688
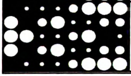	2206	70.33	1.93E+01	0.687

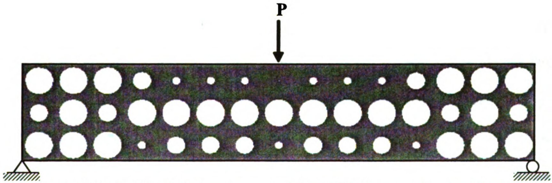

Figure 3-14. Optimal design generated for MBB-beam using the discrete variable set

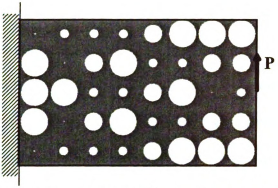

Figure 3-15. Optimal design generated for the 8-bar truss using the discrete variable set

3.3.6 Validation of Optimal Solutions

To ensure proper functionality of the proposed optimization technique, the optimal solutions to the MBB-beam and 8-bar truss problems (Figure 3-14 and Figure 3-15) were compared to those obtained with two well-established topology optimization techniques. Specifically, the optimal solutions generated by employing: the numerical multiresolution approach and a power-law approach were examined (see Chapter 2).

The multiresolution approach proposed by Chellappa et al. (2004) also evaluated solutions to the MBB-beam and 8-bar truss problems. Thus, these results are used as one set of benchmark solutions to compare the optimal design obtained by the proposed approach in this thesis. The optimal solutions obtained through implementation of the proposed parametric approach compare favorably to those achieved by Chellappa et al. (2004) through their multiresolution technique. A visual comparison of the optimal solutions for the MBB-beam shows that the material layout in both solutions is quite similar (Figure 3-16 and Figure 3-17). Upon analyzing the respective optimal structures computationally (i.e. performing finite element analysis), it was found that minor variations do exist in the resulting mass, strain energy, and deflection (or compliance). A summary of results is given in Table 3-8. The relative density of the MBB-beam obtained using both approaches were identical. However, a 5% difference was observed in the compliance and strain energy.

The optimal material layouts and analytical results for the 8-bar truss were also compared (Figure 3-18 and Figure 3-19). Again, a visual comparison indicates that the obtained solutions have similar material distributions. Similar to the MBB-beam comparison, the analytical results for the 8-bar truss varied minimally between the two optimization approaches. The comparison of results for the 8-bar truss problem is given in Table 3-9. Similar to the results obtained by the MBB-beam, the relative density of the 8-bar truss obtained using both approaches were identical. However, an 8% difference was observed in the compliance and strain energy.

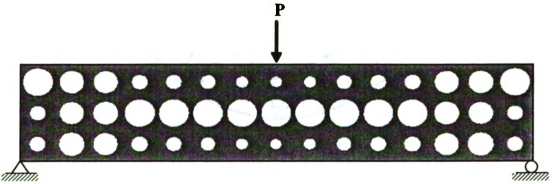

Figure 3-16. Optimal solution for MBB-beam using the multiresolution approach by Chellappa et al. (2004)

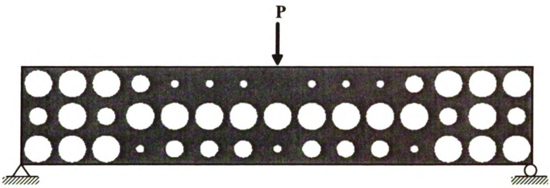

Figure 3-17. Optimal solution for MBB-beam using the proposed parametric modeling approach

Table 3-8. Comparison in results for the MBB-beam

	Parametric Modeling Approach (A)	Multiresolution Approach (B)	(A/B)
Relative Density	0.65	0.65	0.0
Compliance	72.20	69.06	5.0
Strain Energy	36.10	34.53	5.0

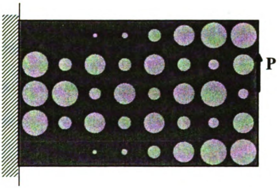

Figure 3-18. Optimal solution for 8-bar truss using the multiresolution approach by Chellappa et al. (2004)

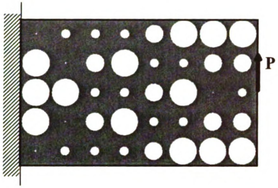

Figure 3-19. Optimal solution for the 8-bar truss using the proposed parametric modeling approach

Table 3-9. Comparison in results for the 8-bar truss

	Parametric Modeling Approach (A)	Multiresolution Approach (B)	(A/B)
Relative Density	0.70	0.70	0.0
Compliance	38.55	35.67	8.0
Strain Energy	19.27	17.84	8.0

The material distributions obtained for both the MBB-beam and the 8-bar truss through the parametric procedure and the multiresolution approach were quite similar. Material was shifted so as to transfer the load directly to the supports, placing more material in regions of higher stresses and removing material from regions under low stresses. The variation in computational solutions between the parametric modeling approach and the multiresolution approach (Table 3-8 and Table 3-9) were minor and may be due to the differences in the employed optimization techniques and/or the stopping criteria implemented by the two methods. As mentioned previously, Chellappa et al (2004) implemented a multiresolution approach to topology optimization (Chapter 2), which is a gradient-based technique. The search method implemented in gradient-based approaches differs from that of a genetic algorithm (see Chapter 2) (Arora 1989). The stopping criteria implemented in the multiresolution approach also differs from that of the GA. Unlike the multiresolution approach which uses a convergence based stopping criterion, the stopping criterion of this genetic algorithm is based on the number of user defined cycles. In this case, optimization continues until the amount of cycles is completed, however convergence can still be detected. As stated previously, if the fitness value of the last design saved is relatively close to the 2 or 3 designs saved prior, convergence can be assumed. Furthermore, convergence can assumed if the last design saved was found approximately 10 cycles prior to completion of the last cycle.

The power-law approach to topology optimization (Chapter 2) proposed by Bendsöe was also implemented to generate an optimal topology for the MBB-beam and the 8-bar truss. The power-law technique is capable of optimizing topology problems by distributing an initial amount of material in the design domain such that the compliance of a structure is minimized, i.e., maximum stiffness (Sigmund and Tcherniak 2001). The power-law method is implemented with mesh generation routines and finite element analysis algorithms to perform topology optimization. The optimal solutions generated for both validation problems using an educational version of a topology program that uses the power-law approach (Sigmund and Tcherniak 2001) are displayed in Figure 3-20 and Figure 3-21.

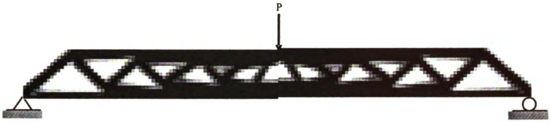

Figure 3-20. Optimal design for MBB-beam problem using a power-law approach

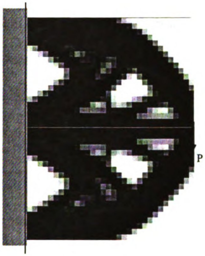

Figure 3-21. Optimal design for 8-bar truss problem using a power-law approach

When comparing the solutions in Figure 3-20 and Figure 3-21 to those obtained through parametric and multiresolution techniques (Figure 3-16-Figure 3-18), it can be noticed that the optimal material distributions are displayed differently. The power-law approach to topology optimization created truss-like optimum structures, while the other two techniques achieved a similar structure through finite, i.e., well-defined, geometric features. As discussed in Chapter 2, unlike the proposed parametric approach to optimization, the power law approach has the advantage of distributing material by addition or removal of cavities within the domain, allowing for more detailed and complex geometries (Haftka and Gurdal 1993). The multiresolution approach can also achieve this by means of coupon libraries with multiple cavities and void coalescence algorithms. The disadvantage of the fine material distribution in the power law solutions, however, becomes apparent when optimizing systems with multiple load cases, boundary conditions, constraints, and objective functions. In order to incorporate these changes, code modification is required (Sigmund and Tcherniak 2001). Furthermore, since solutions may feature complex geometries, modifications or "smoothing" of the optimal design is usually necessary to reduce difficulties in manufacturing.

3.4 Optimization of Continuous Panel Systems-Case Study

The proposed parametric optimization procedure is considered valid based on the comparisons with established topology optimization techniques in the previous section. The parametric approach is now applied in this section within the context of a specific problem, a continuous panel system. The goal for this case study was to optimize the material/structural layout of the transverse cross-section of a continuous panel system for maximum stiffness using the proposed parametric modeling approach. Specifically, the continuous panel system will be defined as a bridge deck with multiple, equally spaced supports. The following sections introduce and discuss the problem definition, parametric modeling and optimization problem formulation, and optimization results in detail.

3.4.1 Problem Definition

The case study was performed by optimizing the material distribution within the transverse cross-section of a continuous panel system (i.e. bridge deck). The geometric domain and loading and boundary conditions are discussed in further detail throughout this section.

The optimization process was formulated for a bridge deck continuous panel system subjected to concentrated loads, P, at the midspan of each bay (Figure 3-22). The supports or girders of bridge deck are equally spaced at 6 ft apart. The deck is designed with a thickness of 6 in. This system experiences moving loads, and thus was designed for the maximum case scenario which is a point load at each span (Figure 3-23). The loading condition displayed in Figure 3-22 is experienced by an effective width along the length of the system. For bridge decks on girders, such effective width can be determined from code recommendations (Barker and Puckett 1997). It is suggested that the effective width be calculated using the following equations: (1) for the region experiencing a positive moment, S_w^+=26.0+6.60S and (2) for the region experiencing a negative moment, S_w^- = 48.0+3.0S; where, in both cases, S is the spacing between supports in feet.

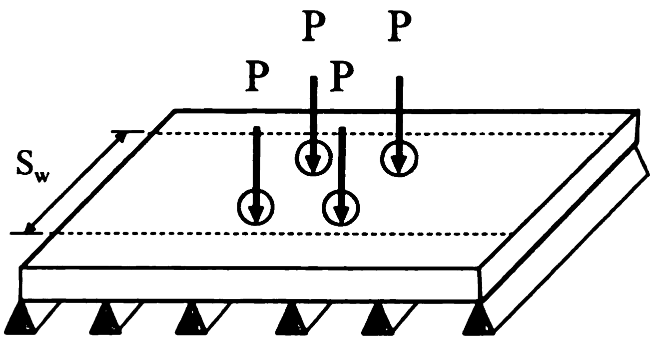

Figure 3-22. Loading and boundary conditions of entire system

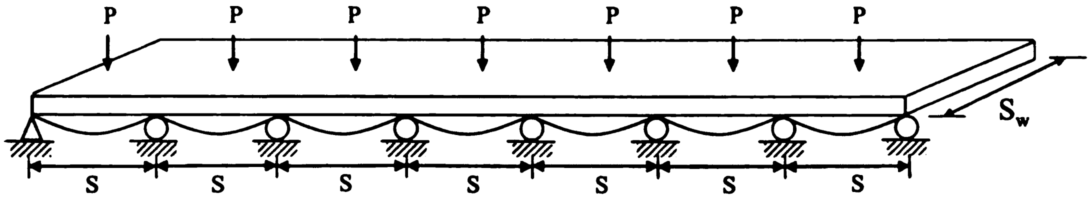

Figure 3-23. Deformation of continuous panel system

A bridge deck is a three-dimensional complex system and simplifications are necessary for modeling purposes. Due to the periodic boundary conditions, modeling of the entire bridge deck was simplified into a single representative span (see Figure 3-24). Furthermore, the structure and loading conditions are symmetric about that span, allowing for further simplification as shown in Figure 3-25.

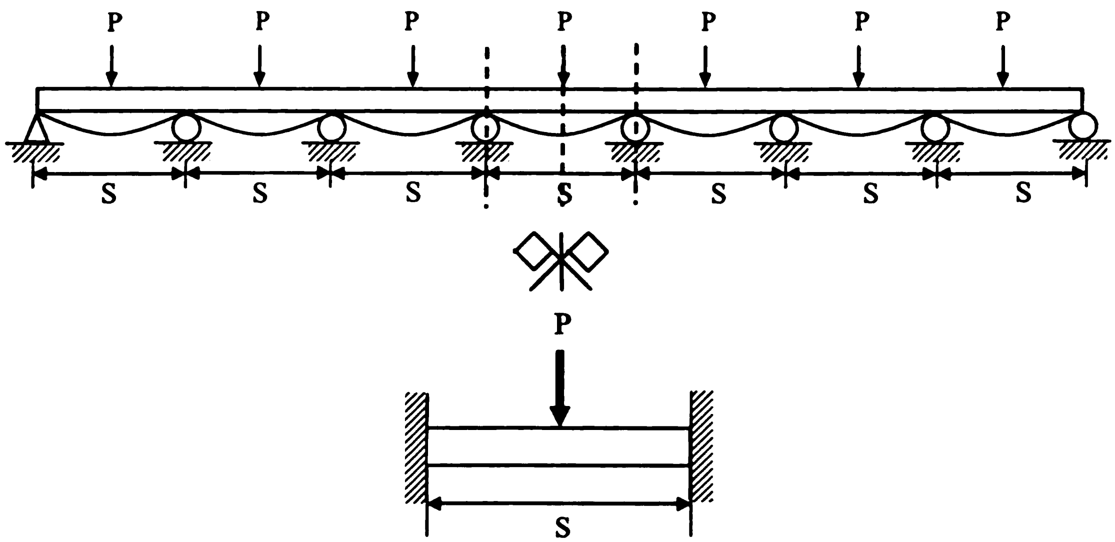

Figure 3-24. Representative span due to periodic boundary conditions

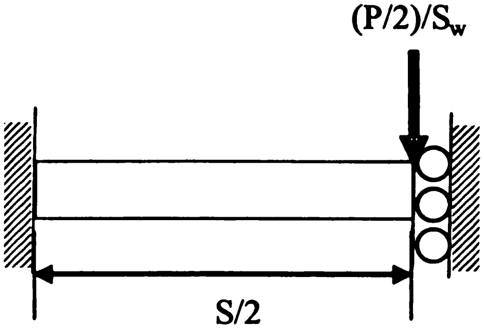

Figure 3-25. Simplified model of continuous panel system due to symmetry

The applied load on the system was defined as that produced by one wheel of a design truck. Bridge design specifications state that the wheel load of a design truck without impact is 16 kips. This load is transmitted to the deck system over a longitudinal effective width, S_w (Barker and Puckett 1997). In this case, since the load was applied to the region experiencing the positive moment, the effective width was determine using, $S_w^+=26.0+6.60S$. The bridge deck continuous panel system has a spacing of 6 ft between girder supports, resulting in an effective width, S_w, of approximately 66 inches. Since the load is applied at the symmetry line, only half of it is considered. Thus, the load per unit width of longitudinal deck was equal to 8 kips/ 66 in. = 121.2 lbs/in.

3.4.2 Parametric Modeling and Optimization Problem Formulation

Like the validation procedure, the simplified structure displayed in Figure 3-25 was modeled with an initial hierarchy and the optimization was conducted using a parametric approach as shown in Figure 3-26. The radii of each void were defined as the controlling parameters and their size change essentially modified the material distribution within the domain.

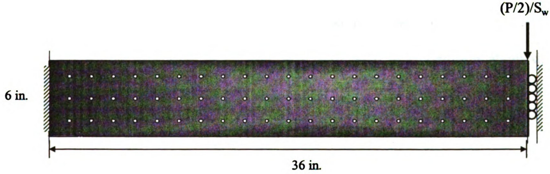

Figure 3-26. Parametric model (initial design)

The optimization problem formulation implemented for the continuous panel was more complex than that used for the validation process. Unlike the validation problem formulations, multiple design variables and constraints were implemented for optimization.

In order to define the design variables for the continuous panel system, it was necessary to discretize the initial designs into small rectangular virtual elements. As mentioned previously, these elements were created to assist in defining variable sets for the controlling parameters which were the void radii. The model was discretized into fifty-three 1.71 in. × 2.0 in. virtual regions (see Figure 3-27). Similar to the validation procedure, each void was numbered so that a corresponding radius could be defined. The voids in the upper left hand corner of Figure 3-26 was assigned a corresponding radius of r_1, and continued along the rows, completing with the void in the lower right hand corner which was identified as having a radius of r_{63}.

Discrete and dependent variables were defined in the formulation. The discrete variable sets were identified such that each void could increase to a maximum radius of 0.835 in. to prevent overlapping and/or exceeding the pre-defined domain. Since the structure is expected to exhibit a symmetric bending moment distribution along its length, dependent variables were defined to enforce a line of symmetry along a "diagonal". This implies a symmetry line condition about the middle of the bean subjected to an 180° rotation.

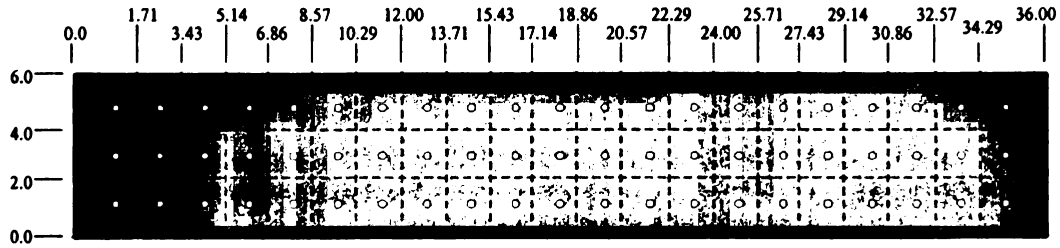

Figure 3-27. Virtual regions surrounding each void in the initial design (dimensions shown in inches)

The simplified panel system was subjected stress, strain, deflection, and mass constraints. The deflection constraint was determined by using the standard conditions and regulations of bridge deck design. Using a code recommendation for a bridge deck, deformations were limited to *S*/800 (Barker and Puckett 1997). In this case, *S* is defined as the distance between bridge supports, 72 in., resulting in a maximum allowable deflection of .09 inches.

As discussed previously, the motivation of this research was to use natural fiber composites for load-bearing applications (Chapter 1), thus, the stress and strain constraints were determined for randomly oriented, short fiber composites, specifically, industrial green hemp/unsaturated polyester (UPE) composite systems. The longitudinal strain constraint was determined from the longitudinal stress assuming a linear elastic isotropic material. Halpin and Pagano (1996) developed approaches to determine equivalent isotropic elastic constants for randomly oriented fiber composites by approximating the composite as a quasi-isotropic laminate (Gibson 1994, Quagliata 2003). Defining the isotropic modulus of a randomly oriented fiber composite is accomplished by assuming the composite consists of various superimposed unidirectional layers, each layer characterized by its fiber orientation and with layer behavior being fully additive over all layers. Therefore, the elastic modulus can be modeled by geometrically averaging the properties of the unidirectional layers over all fiber orientations (Gibson 1994). The "average" isotropic elastic modulus for randomly oriented, industrial green hemp/UPE composites was evaluated experimentally through material testing in previous research by Quagliata (2003) to be 900,000 psi, which is approximately half that of a randomly distributed chopped-strand-mat E-glass composite.

The maximum allowable longitudinal stress, σ_{11} was also determined using results from previous research obtained through ultimate tensile strength (UTS) testing for biocomposite systems. Testing of the industrial green hemp/UPE composite samples withstood, on average, a maximum stress of approximately 3 ksi (Quagliata 2003). Incorporating a factor of safety of 2, the maximum longitudinal stress was limited to 1.5 ksi. Furthermore, a Von Mises stress constraint was set to $.577\sigma_{max}$ to limit shear-induced failures, obtaining a maximum allowable value of 865.75 psi. Assuming a linear elastic material, an ultimate longitudinal strain of .0033 can be back calculated from the ultimate tensile strength and the modulus obtained from previous material testing. Incorporating a factor of safety of 2, the allowable longitudinal strain was defined as 1.65e-4.

Lastly, the mass constraint was identified by defining the system's relative density. Specifically, the mass of the optimized design should be 7/10 that of the solid structure, that is, a $\rho_{relative}$ of 0.70.

Like the validation formulation for the MBB-beam and the 8-bar truss, the continuous panel system was optimized using strain energy as the objective function since the overall goal is to obtain the stiffest possible design. Stiffness is chosen as the main design objectives since it usually governs the design of fiber reinforced polymer composites, and consequently any designs to be made from natural fiber reinforced polymer composites. Therefore, the goal was to minimize the overall structural strain energy while simultaneously satisfying all design constraints. Again, due to the indirect relationship between mass and strain energy, mass was the primary governing constraint. Thus, it was necessary for the optimizer to locate a design that was light enough to minimize the strain energy, but not too light that constraints were violated. Table 3-10 and Table 3-11 outline the problem formulation used for optimization of the simplified continuous panel system. This formulation was defined in the optimizer prior to process initiation.

Table 3-10. Optimization problem formulation for the simplified continuous panel system

Find:	r_n, where n = void number = 1-32 (integers)
That minimizes:	Strain Energy
Subject to:	Mass constraint Stress constraint Strain Constraint Deformation Constraint

Find:	r_n, where n = void number 1-32 (integers)
That minimizes	$f(x) = \int_V \sigma\varepsilon \, dv$
Subject to:	$g_i(x) \leq 0$, i = 1- n constraints $h_i(x) \geq 0$, i = 1- n constraints

Table 3-11. Summary of formulation elements for the simplified continuous panel system

Formulation Elements	Variable Type	Definition of Formulation Element	
Design Variables	Discrete	Void Radii	r_n, where n = void number = 1-32 (integers)
	Dependent	Void Radii	r_n, where n = void number = 33-63 (integers)
	Parameter	Length	L
	Parameter	Height	H
Constraints		Maximum Allowable Longitudinal Stress	$\sigma \leq 1500$ psi
		Minimum Allowable Longitudinal Stress	$\sigma \geq -1500$ psi
		Maximum Allowable Von Mises Stress	$\sigma \leq 865.5$ psi
		Minimum Allowable Von Mises Stress	$\sigma \geq -865.5$ psi
		Maximum Principal Strain	$\varepsilon \leq .00165$
		Minimum Principal Strain	$\varepsilon \geq -.00165$
		Allowable Deformation	$\delta \leq .09$ in.
		Mass	$M \leq 151.20$ lbs
Objective Function		Minimize Strain Energy	

As stated in previously, a fitness function was used to determine the optimality of the design solutions generated by the genetic algorithm for this case study. The fitness value was dependent on the objective function and the design constraints. The fitness function defined in the optimizer, HEEDS, for this case study was as follows:

$$f = \frac{E}{NormalizingCoefficient} - [10{,}000 * \begin{pmatrix} (M_{allowable} - M_{violated}) - \\ (\sigma_{allowable} - \sigma_{violated}) - \\ (\varepsilon_{allowable} - \varepsilon_{violated}) - \\ (\delta_{allowable} - \delta_{violated}) \end{pmatrix} \quad (3.3)$$

This function was evaluated by HEEDS at the end of each design iteration and the fitness level of the design is dependent the obtained value. The last design saved had the highest fitness value and was considered optimal if the fitness value of the prior designs was similar to the last design obtained or the last design obtained was found approximately 10 cycles prior to completion of the last cycle.

3.4.3 Implementation of Optimization Process and Evaluation of Optimal Solutions

Using the problem formulation given in Table 3-10, the formulation elements shown in Table 3-11, and the parametric model displayed in Figure 3-26, the proposed optimization procedure was implemented to optimize the transverse cross-section of the continuous panel system in Figure 3-25. The material distribution within the cross-section was optimized twice, each time with a modified discrete variable set. The first attempt was implemented with a discrete variable set consisting of 17 values where the void radii ranged from 0.05 to 0.835 inches in increments of .05. The second optimization trial was performed with a much smaller discrete variable set, where of only 4 void radii values between 0.05 inches and 0.835 inches were possible. The decreased variable set size was implemented to reduce manufacturing difficulties in creating random size voids. The results obtained from both optimization trials were compared to observe if variation in solutions existed when accounting for manufacturing constraints.

Throughout the early stages of optimization an immediate or consistent decrease in strain energy was not observed. As noted in Figure 3-28 and Figure 3-29, the optimization history exhibited an oscillatory nature due to the stochastic search method of the G.A. and also the fact the fitness value for all designs is not solely dependent on the objective function, but is also dependent on the constraint violations. However, as the designs evolved (Table 3-12 and Table 3-13) the reduction in strain energy was more consistent in the newer designs and an optimum was found. The design solutions obtained satisfied all design constraints (Figure 3-30 through Figure 3-34) while simultaneously achieving adequate strain energy. The last designs generated and saved by HEEDS for the panel system had the highest fitness values and were considered optimal since both were obtained approximately 10 cycles before completion of the 75th or last cycle. The designs generated are shown in Figure 3-35 and Figure 3-36 for the increased and decreased discrete variable sets, respectively.

Figure 3-30 through Figure 3-34 display the constraint history for the case study optimized with the increased discrete variable set. The mass constraint history is shown in Figure 3-30. . This constraint was violated through the majority of the optimization procedure; however, as the design numbers increased the mass approached the maximum allowable value of 151.2 lbs. The mass constraint was met by design 2386 at an approximate cycle number of 60. When examining the plot, it may look like design 2386 was the last to be generated by HEEDS which makes satisfying the constraint look like a coincidence; however, since the cycle number was set to 75, the search for a "better" solution continued until the last cycle had completed and was not found. Figure 3-31 displays the behavior of the deflection constraint which remained less than the maximum allowable value of .09 in. throughout the entire optimization process. The behaviors of the longitudinal and Von Mises stresses are shown in Figure 3-32 and Figure 3-33. Similar to the structure's deflection, large stress concentrations did not seem to be an issue; thus, the stress constraints were not violated. The strains experienced by the designs generated throughout the optimization process (Figure 3-34) were also much less the maximum allowable value of .0033.

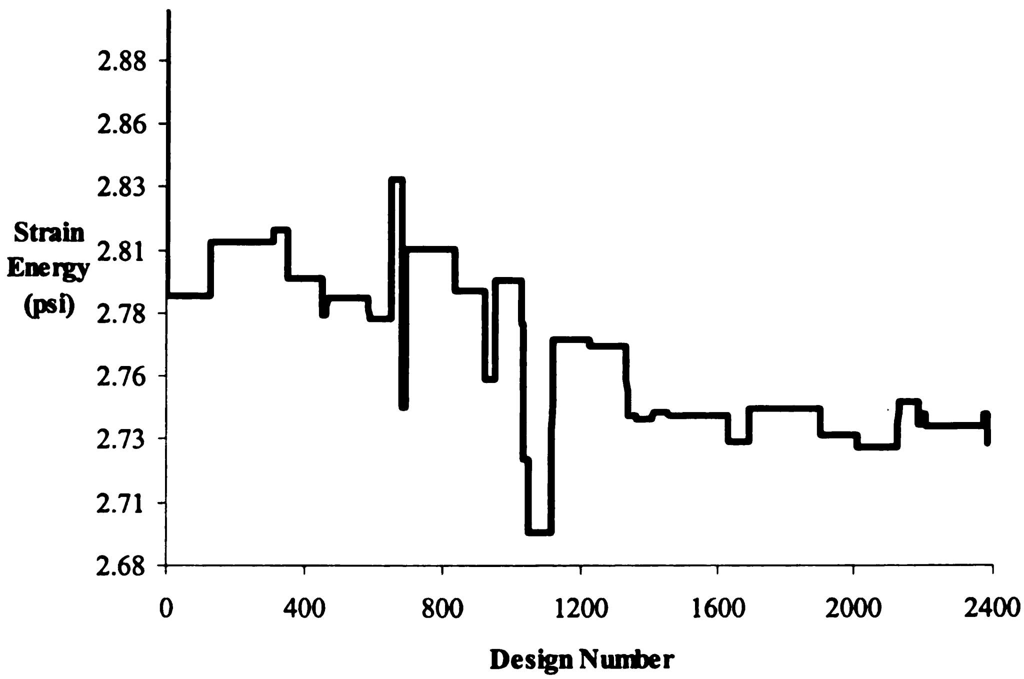

Figure 3-28. Optimization history of continuous panel system with increased discrete variable set

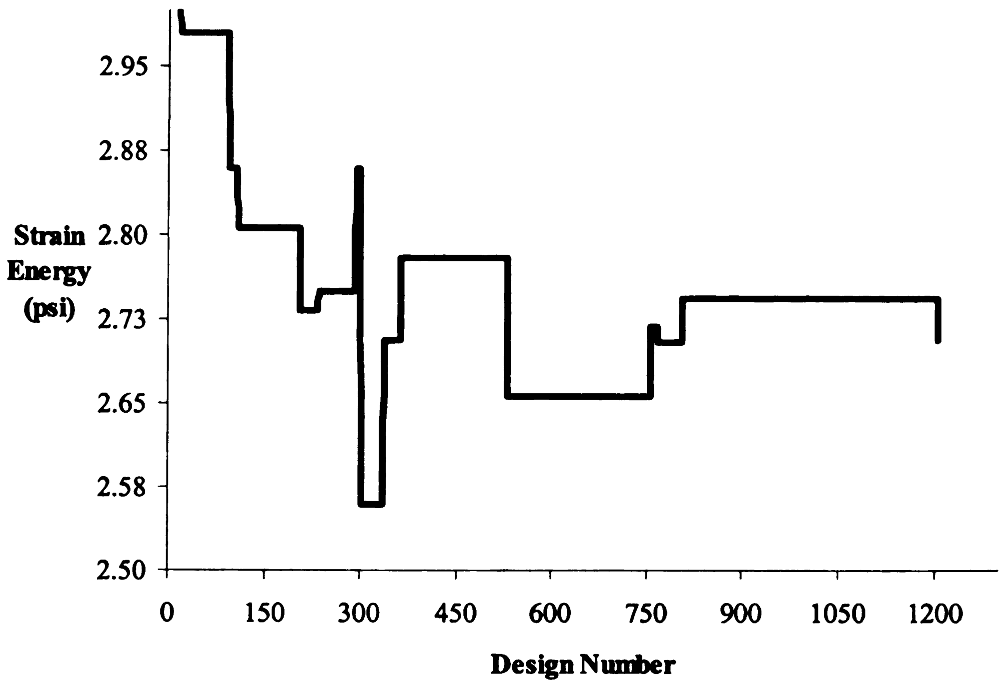

Figure 3-29. Optimization history of continuous panel system with decreased variable set to account for manufacturing

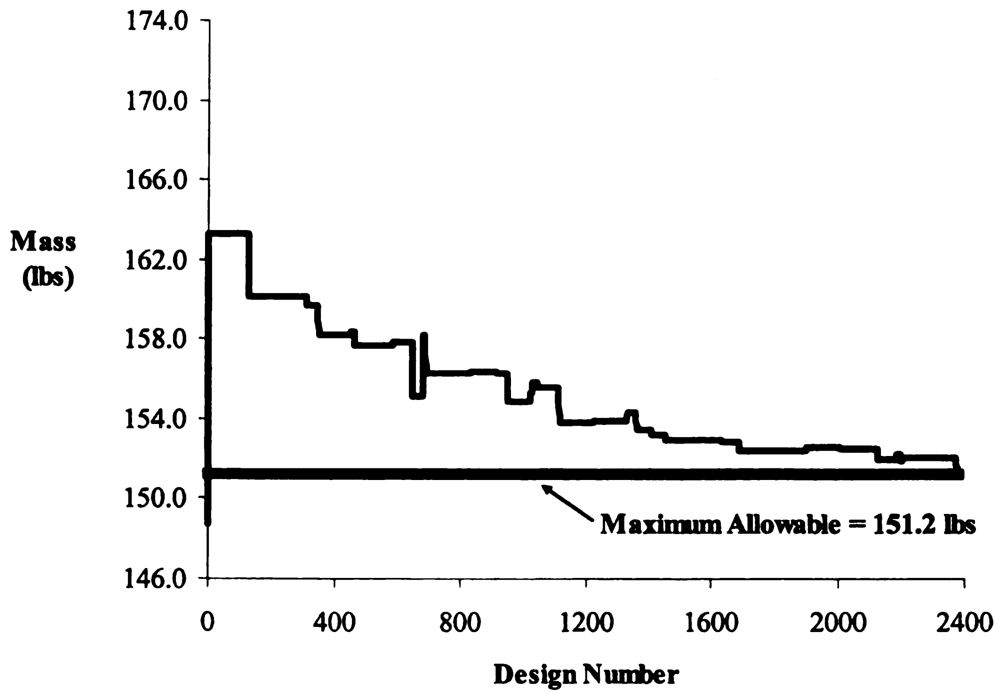

Figure 3-30. Mass constraint history evaluation

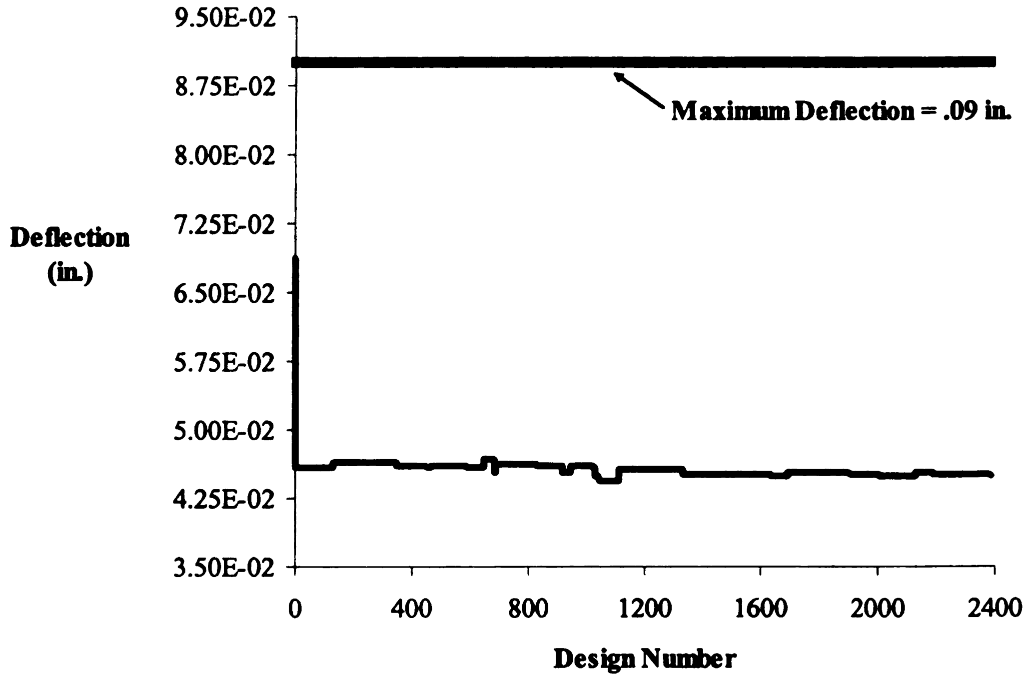

Figure 3-31. Deflection constraint history evaluation

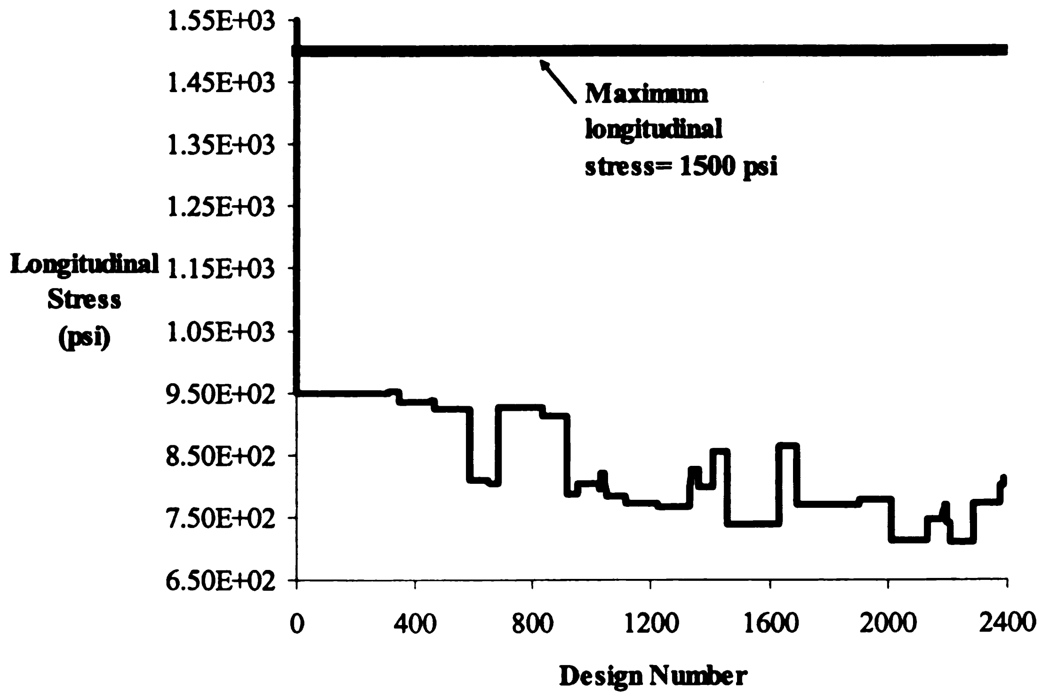

Figure 3-32. Longitudinal stress evaluation history

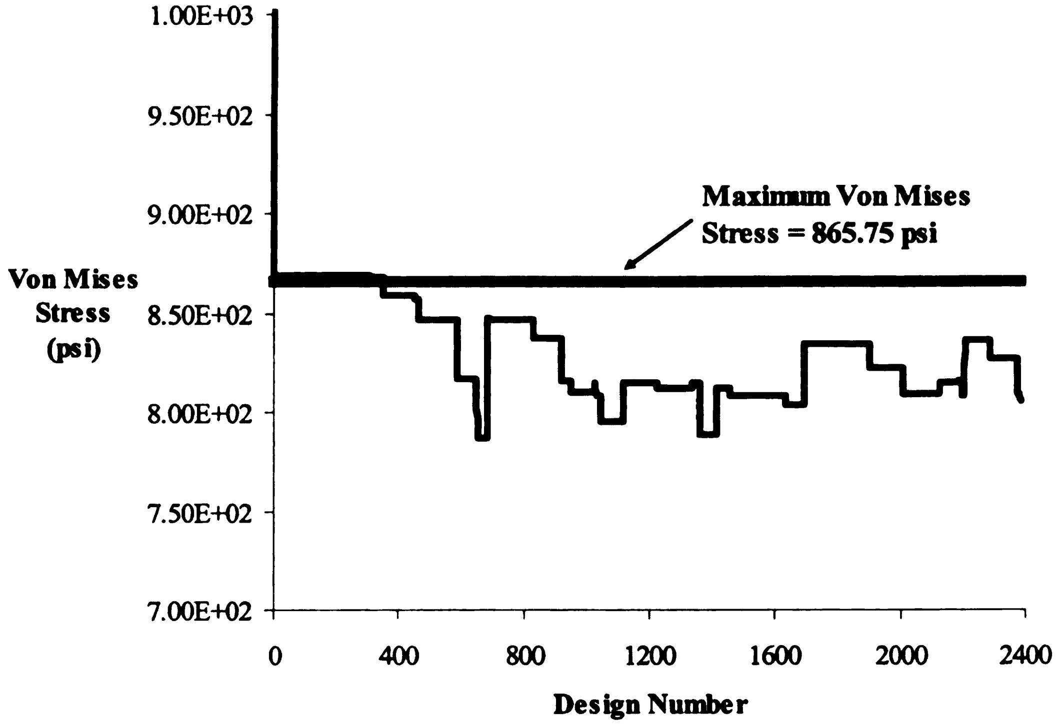

Figure 3-33. Von Mises stress evaluation history

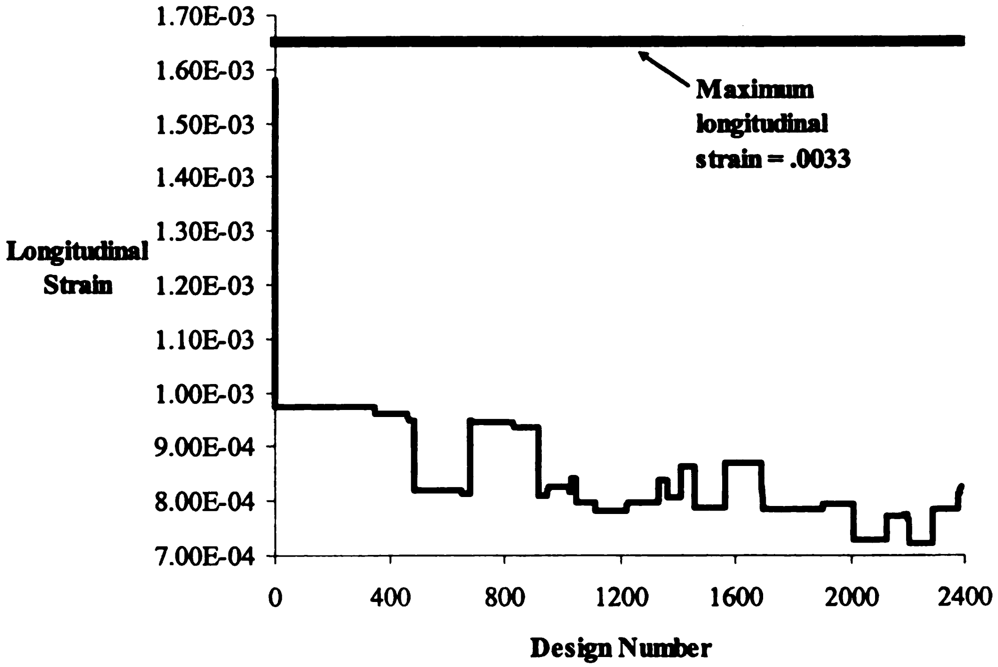

Figure 3-34. Longitudinal strain evaluation history

Table 3-12. Evolution of designs for case study with increased discrete variable set

Design	Design Number	Mass (lbs)	Deflection (in)	Strain Energy (psi)	Relative Density
	1	148.69	6.87E-02	4.16E+00	0.688
	2	163.29	4.59E-02	2.79E+00	0.756
	129	160.14	4.64E-02	2.81E+00	0.741
	312	159.73	4.64E-02	2.81E+00	0.739
	350	158.17	4.61E-02	2.79E+00	0.732
	454	158.35	4.59E-02	2.78E+00	0.733
	466	157.66	4.60E-02	2.79E+00	0.730
	588	157.85	4.59E-02	2.78E+00	0.731
	651	155.13	4.68E-02	2.83E+00	0.718
	683	158.23	4.53E-02	2.74E+00	0.733
	691	156.30	4.63E-02	2.81E+00	0.724
	833	156.35	4.60E-02	2.79E+00	0.724
	919	156.28	4.54E-02	2.75E+00	0.724
	952	154.83	4.61E-02	2.79E+00	0.717
	1026	155.34	4.58E-02	2.78E+00	0.719
	1031	155.81	4.49E-02	2.72E+00	0.721
	1047	155.58	4.44E-02	2.69E+00	0.720
	1117	153.80	4.57E-02	2.77E+00	0.712
	1224	153.86	4.57E-02	2.77E+00	0.712
	1335	154.36	4.52E-02	2.74E+00	0.715
	1363	153.47	4.52E-02	2.74E+00	0.711
	1412	153.18	4.52E-02	2.74E+00	0.709
	1457	152.96	4.52E-02	2.74E+00	0.708
	1633	152.84	4.50E-02	2.73E+00	0.708

Table 3-8. Evolution of designs for case study with increased discrete variable set (cont.)

Design	Design Number	Mass (lbs)	Deflection (in)	Strain Energy (psi)	Relative Density
	1692	152.37	4.53E-02	2.74E+00	0.705
	1902	152.60	4.51E-02	2.73E+00	0.706
	2008	152.50	4.50E-02	2.73E+00	0.706
	2128	151.97	4.53E-02	2.75E+00	0.704
	2187	152.27	4.51E-02	2.74E+00	0.705
	2198	151.86	4.52E-02	2.74E+00	0.703
	2207	152.07	4.51E-02	2.74E+00	0.704
	2287	152.05	4.51E-02	2.74E+00	0.704
	2375	151.35	4.51E-02	2.74E+00	0.701
	2386	151.76	4.50E-02	2.73E+00	0.703

Table 3-13. Evolution of designs for case study with decreased variable set to account for manufacturing

Design	Design Number	Mass (lbs)	Deflection (in)	Strain Energy (psi)	Relative Density
	1	154.43	6.30E-02	3.83E+00	0.715
	2	164.35	4.90E-02	3.01E+00	0.761
	18	159.30	4.90E-02	2.98E+00	0.738
	95	164.55	4.70E-02	2.86E+00	0.762
	109	161.75	4.60E-02	2.81E+00	0.749
	206	162.48	4.50E-02	2.73E+00	0.752
	235	162.12	4.50E-02	2.75E+00	0.751
	293	159.27	4.70E-02	2.86E+00	0.737
	301	162.13	4.20E-02	2.56E+00	0.751
	337	160.57	4.46E-02	2.71E+00	0.743
	363	157.90	4.59E-02	2.78E+00	0.731
	531	154.75	4.38E-02	2.66E+00	0.716
	757	154.21	4.48E-02	2.72E+00	0.714
	767	153.29	4.46E-02	2.71E+00	0.710
	806	151.40	4.50E-02	2.74E+00	0.701
	1207	152.09	4.46E-02	2.71E+00	0.704

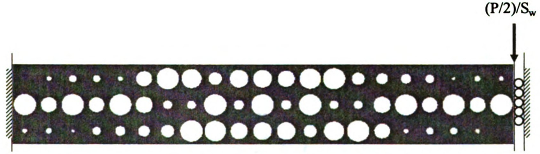

Figure 3-35. Optimal design generated for the continuous panel system using the increased discrete variable set

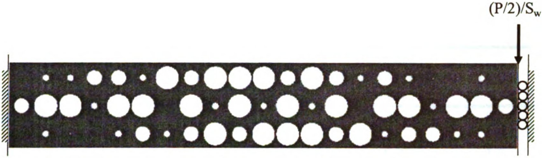

Figure 3-36. Optimal design generated for the continuous panel system with decreased variable set to account for manufacturing

The optimal solutions for the case study presented for the increased discrete variable set formulation in Figure 3-35 and the decreased variables set formulation in Figure 3-36 display similar trends. Material was placed in regions experiencing large stress concentrations, specifically in areas of high tension and compression as illustrated in See Figure 3-37. In both cases the material layout is arranged so as to more efficiently transfer the applied loads to the support conditions. A quantitative comparison of the two design solutions obtained for the cases study is displayed in Table 3-14. The computational results were quite similar displaying only a 1% difference in mass, deflection, and strain energy, a 20% difference in the longitudinal stress, and an 8% difference in the Von Mises stress.

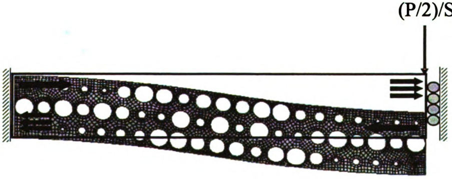

Figure 3-37. Panel Response analysis highlighting

Table 3-14. Summary of results for the designs solutions obtained for the case study

	Increased Discrete Variable Set (A)	Decreased Discrete Variable Set (B)	(A/B)
Relative Density	0.70	0.70	0.0
Mass (lbs)	151	152	1.0
Deflection (in.)	4.50E-02	4.46E-02	1.0
Longitudinal Stress (psi)	813	676	20.0
Von Mises Stress (psi)	806	872	8.0
Strain	8.26E-04	7.40E-04	12.0
Strain Energy (psi)	2.73	2.70	1.0

After examining finite element analysis results for both the initial and optimal designs for the case study, it was apparent the optimized structure exhibited more homogenous stress and strain fields (Figure 3-38 through Figure 3-43) than the initial design. However, the optimal configuration exhibited larger deformations (see Figure 3-44 and Figure 3-45) than the initial design. This difference is a direct consequence of the available material since the initial design has a relative density of 0.98 compared to 0.70 for the optimal, or 40% more material. Nonetheless, the deformation constraint defined in the optimization problem formulation (Table 3-11) was still satisfied. Thus the optimal design is a much more efficient and economical (less material) solution. A comparison in computational results for both the initial and optimal designs is summarized in Table 3-15.

The computational design solution obtained for this case study, using the proposed parametric approach to optimization, was examined further through small-scale component testing. Flexure tests were implemented to study the difference in performance of a base periodic cellular structure and a structure with the optimized material distribution. This experimental portion of this study is introduced and discussed in further detail in Chapter 4.

Figure 3-38. Longitudinal stress field experienced by initial design for the case study

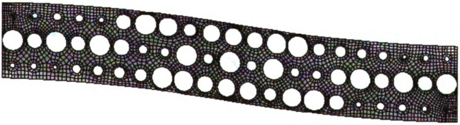

Figure 3-39. Longitudinal stress field experienced by optimal design obtained for the case study

Figure 3-40. Von Mises stress field experienced by initial design obtained for the case study

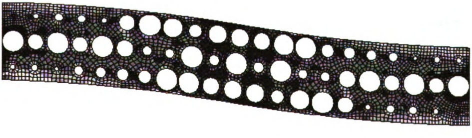

Figure 3-41. Von Mises stress field experienced by optimal design obtained for the case study

Figure 3-42. Strain field experienced by initial design for the case study

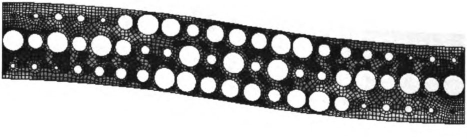

Figure 3-43. Strain field experienced by optimal design obtained for the case study

Figure 3-44. Deformation experienced by initial design for the case study

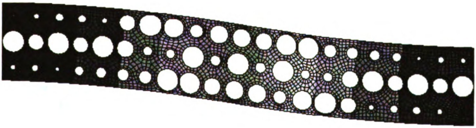

Figure 3-45. Deformation experienced by optimal design obtained for the case study

Table 3-15. Comparison in computational results for the initial and optimal designs for the case study

	Optimal Design (A)	Initial Design (B)	(A/B)
Relative Density	0.70	0.98	40.0
Mass (lbs)	151.00	213.00	41.0
Deflection (in.)	0.045	0.030	50.0
Max. Longitudinal Stress (psi)	813.00	448.00	81.0
Max.Von Mises Stress (psi)	806.00	1158.00	44.0
Max. Strain	8.26E-04	6.23E-04	33.0
Strain Energy (psi)	2.73	1.84	48.0
Strain Energy/Mass (psi/lbs)	0.018	0.009	209.0

4 EXPERIMENTAL VALIDATION

4.1 Overview

The findings from the computational studies were used to assess the feasibility of natural fiber composites for load-bearing applications through small-scale component testing. This chapter provides an account of the manufacturing and experimental testing of an optimal and a non-optimal biocomposite panel system built using industrial green hemp and unsaturated polyester resin (UPE). The small-scale cellular samples fabricated this study: (1) a base periodic cellular design for the continuous panel system and (2) the generated optimal hierarchical cellular solution. Both samples were fabricated using the vacuum assisted resin transfer molding (VARTM) manufacturing method and their performance was evaluated through flexural testing.

4.2 Material Systems and Structural Forms

This section discusses in detail the material and resin systems, as well as the structural forms implemented for the experimental study. In order to obtain a higher performance natural fiber composite, a hybrid material system in multiple advanced structural configurations were fabricated. The hybrid natural fiber system used for this experimental study and was comprised of jute and industrial green hemp (Figure 4-1). The jute fabric consisted of Hessian jute mats (IJIRA, Calcutta, India), which was used as a face sheet. The industrial green hemp fibers (Flaxcraft, Inc., Cresskill, NJ) were random chopped fibers with average length of 0.3 to 0.5 inches and an aspect ratio (*L/d*) of 100, which were used to make up the core of the sample (Figure 4-2).

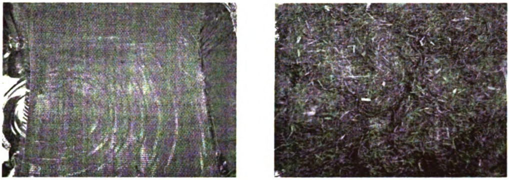

(a) Jute mat (b) Green hemp short fibers

Figure 4-1. Pictures of natural fibers used for fabrication

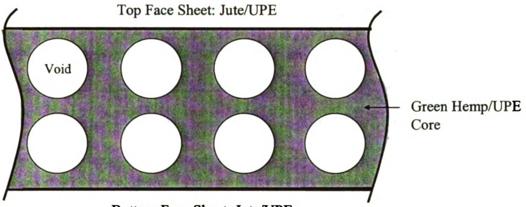

Figure 4-2. Arrangement of hybrid natural fiber material system

The resin system employed for fabrication of the biocomposite cellular samples was orthounsaturated polyester (UPE) resin (Kemlite Co., Inc., Joliet, IL) with a methyl ethyl ketone peroxide (MEKP, Sigma Aldrich) catalyst, and cobalt naphthenate (CoNAP, Sigma Aldrich) promoter. The resin system composition is shown in Table 4-1.

Table 4-1. Resin System

Constituent	Amount by Weight	% by Resin Weight
UPE (33% Styrene)	1000 g	--
MEKP	1.5 g	0.15
CN	0.3 g	0.03

The natural fiber and resin materials discussed in the previous paragraphs were used to create two test samples, namely a base and an optimal design. The geometry and material layout of the base and optimal panel system for verification of the design case study are shown in Figure 4-3. The designs displayed in Figure 4-3 have larger dimensions than that displayed by the initial and optimal design solutions presented in Section 3.4.2. This is because the initial and optimal designs for the case study were fabricated to simulate the entire distance between supports (Figure 3-24) with a segment of overhang. This was done for testing purposes, and will be addressed in the following sections.

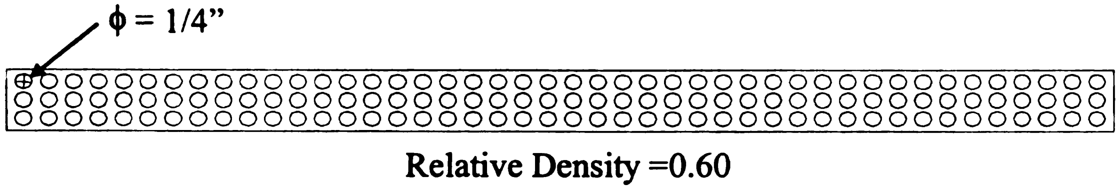

(a) Base periodic cellular design

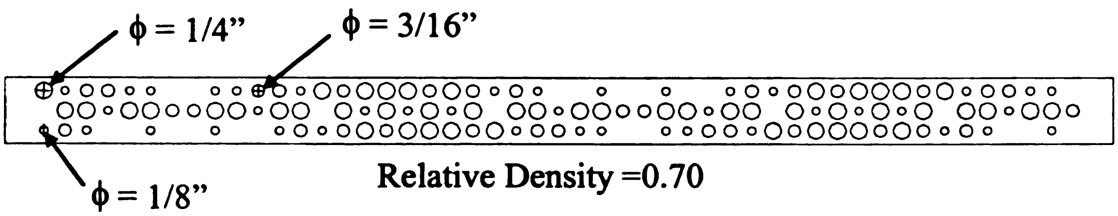

(b) Optimal design obtained through parametric modeling

Figure 4-3. Test unit dimensions and cross-sectional geometry of cellular biocomposite panels (16 × 3 × 1 inches)

4.3 Automated Manufacturing Process

This section presents the processing technique implemented for fabrication of the cellular biocomposite samples. In principle, the processing methods available for natural fiber composites can be similar to those for glass fiber composites. Several processes exist such as traditional hand lay-up techniques, autoclaving, compression molding, sheet-molding compound (SMC), and resin transfer molding. However, vacuum assisted resin transfer molding (VARTM) has been shown to be an effective process for fabrication of both glass fiber and natural fiber composites (Brouwer 2000, Quagliata 2003).

VARTM is a clean closed mold manufacturing technique that can be used for the fabrication of natural fiber composites. The use of a closed mold has made this process environmentally safe since it constrains hazardous styrene emission from the resin. VARTM has also proven to decrease cost in comparison to traditional hand lay-up or autoclaving techniques due to reduced labor and low equipment cost. It is possible to perform tailored lay-up and achieve high fiber volume contents through VARTM (Brouwer 2000, Brouwer 2003). The VARTM process involves the placement of dry fibers into a mold and then enclosing the mold with its other half or with vacuum bagging film. After an airtight seal is obtained by this enclosure the resin can then be injected by the use of vacuum pressure. A schematic of a VARTM process is shown in Figure 4-4.

For laboratory scale samples, a VARTM setup can be implemented on a movable cart with two shelves. The sample setup can be arranged in the top shelf while the bottom shelf is used to hold the vacuum pump. A picture of an actual laboratory VARTM setup is shown in Figure 4-5

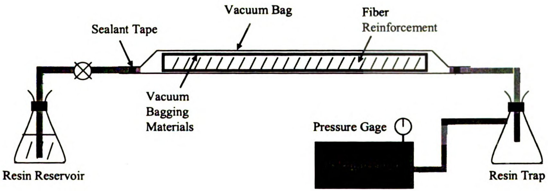

Figure 4-4. Schematic of VARTM manufacturing process

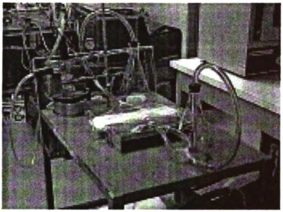

Figure 4-5. Actual VARTM setup

4.3.1 Manufacturing of VARTM Cellular Panels

The automated manufacturing of cellular biocomposite panels was performed using the VARTM process discussed in the previous section (Figure 4-4). This technique was studied experimentally to show that VARTM is a viable technique for manufacturing cellular components with biocomposites. This study included the manufacturing two cellular samples (Figure 4-3) with identical material systems (Section 4.2). The aim was to explore the performance of the biocomposite structures with varying degrees of optimal and non-optimal cellular designs, validate the optimization results, and evaluate VARTM as a viable manufacturing method for these designs

The VARTM manufacturing process was divided into four main steps: (1) preparation of vacuum bagging materials, (2) placement of jute fabric face sheet, dry green hemp core fibers, and cells, (3) vacuum bagging the setup, and (4) resin infusion. Each of these steps is discussed in more detail below.

Special vacuum bagging materials were used to assist in resin transfer and easy release of the sample after resin infusion. The bagging materials were positioned to surround the entire sample. Specifically, all materials lined the bottom of the cellular plate mold and were cut long enough to wrap the entire sample. The bagging material included 5 different plies: (1) a non-porous Teflon release ply, (2) a breather ply, (3) a resin transfer media, (4) a polyester peel ply, and (5) a porous Teflon release ply. First, the non-porous Teflon release ply was placed at the bottom of the mold to prevent the sample from sticking to the mold or the vacuum bag after curing (Figure 4-6a). The breather ply was then placed on top the non-porous Teflon release ply to absorb excess resin from the sample (Figure 4-6b). On top of the breather ply was the resin transfer media (Figure 4-6c). This ply was used to assist in resin transfer for uniform distribution of the resin throughout the sample. A layer of polyester peel ply was then placed on top of the transfer media, which allowed for excess resin to be taken out of the sample (Figure 4-6d). Lastly, the porous Teflon release ply was placed on top of the peel ply (closest to the sample) to allow for excess resin flow and to prevent the other bagging materials from sticking to the sample after curing (Figure 4-6e). Note that the materials were cut large enough to wrap around the entire sample.

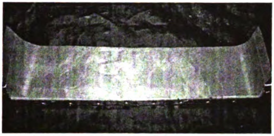

(a) Non-porous Teflon release ply

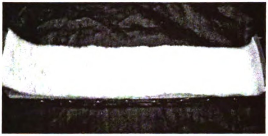

(b) Breather ply

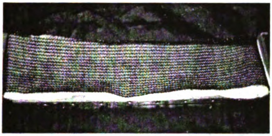

(c) Resin transfer media

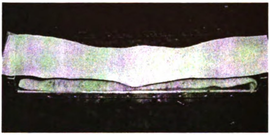

(d) Polyester peel ply

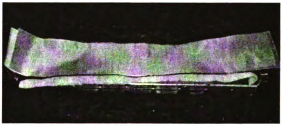

(e) Porous Teflon release ply

Figure 4-6. Picture sequence of vacuum bagging material placement

After all vacuum bagging materials were positioned properly the fibers and cells were ready for placement. First, a jute fabric layer was placed on top of the non-porous Teflon release ply and was cut large enough to longitudinally enclose the entire sample (Figure 4-7a). A layer of green hemp was then uniformly distributed on top of the jute layer as shown in Figure 4-7b. A row of metal rods was then inserted through the mold (Figure 4-7c) to create the first layer of voids. Each metal rod was wrapped with rubber tubing to prevent them from sticking to the sample after curing and thus facilitate their removal. A second layer of green hemp was then placed in between and on top of each rod until they were completely covered (Figure 4-7d).

This process was repeated for all rods layers until all rows of voids were created (see Figure 4-7e).

(a) Layer of jute mat

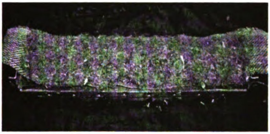

(a) First layer of green hemp fibers

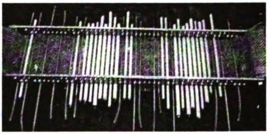

(b) First layer of rods (cell voids)

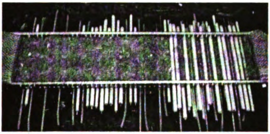

(c) Second layer of hemp fibers and rods

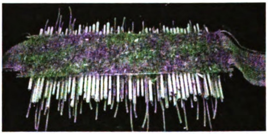

(d) Last layer of hemp fibers

Figure 4-7. Placement of green hemp and rods (void spaces)

The jute and vacuum bagging materials were then wrapped around the green hemp cellular core, ultimately producing a mirror image of the materials on both sides of the sample. (Figure 4-8a and Figure 4-8b).

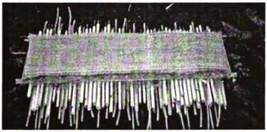

(a) Jute wrapped around green hemp core

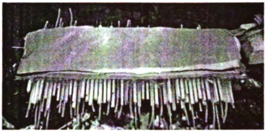

(b) Mirroring of vacuum bagging materials

Figure 4-8. Completed sample ready for bagging

Once they dry sample was in place, a VARTM setup was prepared as shown in Figure 4-4. As previously stated, the setup was implemented on a movable cart with two shelves, one for the sample and the other for the vacuum (see Figure 4-5). Nylon bagging film was cut and placed on the top surface of the cart underneath the mold and was large enough to enclose the entire mold. The resin and vacuum ports were then prepared. A small square wood block, approximately the same height as the mold (1 inch), was used to secure the vacuum port. A strip of sealant tape was placed on top of the block and around the vacuum port and pressed down firmly until stable (Figure 4-9a). The vacuum port was covered with additional breather ply and resin transfer media to improve resin transfer and prevent blocking of the vacuum port. The port was then placed in between the peel ply and resin transfer media on the right edge of the sample. Pieces of breather cloth and resin transfer media were placed around the rods on either side of the mold, around the edges of the mold, and around the wood block to prevent puncturing of the nylon bag (Figure 4-9b). The resin port was created using a vacuum connector. The nylon bagging film was folded on top of the mold to identify the resin inlet. A small puncture was placed in the nylon film toward the left edge of the sample to properly secure a vacuum connector. Once the vacuum connector was properly secured, the bagging film was opened and sealant tape was placed on the vacuum bagging film surrounding the entire mold and also around the vacuum port. Once all materials and ports were in place the sealant tape cover was removed and the nylon bagging film was folded over the entire mold and tightly fastened to the vacuum port and the portion of the bagging film lying on the top surface of the cart. To complete the setup, a valve was added between the resin port and the resin reservoir to control resin flow during resin infusion.

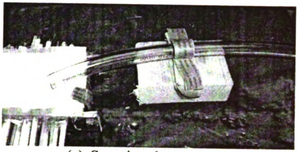

(a) Securing the vacuum port

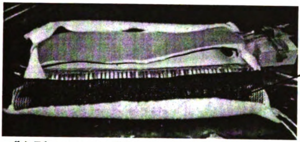

(b) Placement of the vacuum port, breather cloth, and resin transfer media

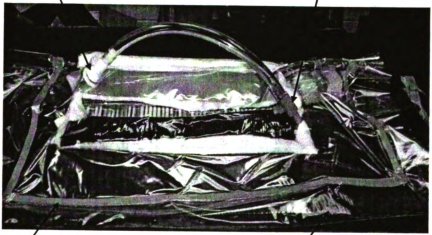

(c) Placement of all ports and sealing of vacuum bag

Figure 4-9. Preparation for resin infusion in the VARTM setup

Lastly, the free ends of the resin and vacuum ports were secured into the resin reservoir and trap (Figure 4-10) and the vacuum pressure was tested to ensure a pressure between 25 and 27 in. of Hg.

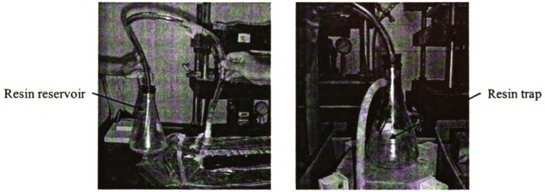

Figure 4-10. Resin and vacuum port attachment to the reservoir and trap

The resin infusion process into the sample began by first compressing the sample under the vacuum pressure for approximately 15 minutes (Figure 4-11). While the dry fibers in the sample were kept under pressure, the polyester resin system was proportioned (see Table 4-1) and added to the resin reservoir. The resin port was secured into the reservoir and the valve was opened to initiate infusion. Initially, the resin moved quickly into the sample. However, after saturation of approximately ¼ of the sample the flow began to slow down saturating the entire sample after approximately 50 minutes. The resin infusion process is shown in Figure 4-12.

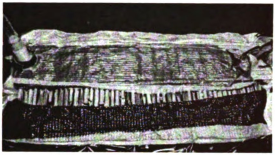

Figure 4-11. Sample under vacuum pressure

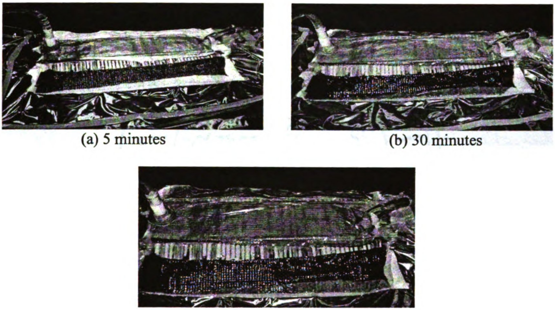

(a) 5 minutes

(b) 30 minutes

(c) 50 minutes

Figure 4-12. Resin infusion process

Once the sample was completely impregnated with resin, the valve between the resin reservoir and the sample was closed so that no additional resin would be pulled into the system. The system was kept under vacuum for approximately 45 minutes to allow the resin to begin gelling and to minimize the amount of air voids that could develop in the sample. After gelling, the vacuum was turned off and the resin and vacuum ports were detached from the mold. The sample was oven cured for

6 hours at 100°C. A lower curing temperature than that used in prior studies (Quagliata 2003) was necessary to avoid melting of the resin transfer media, which is made of polyethylene. Steel plates were placed on top of the sample during curing to assist in creating uniformity on the sample surfaces, squeeze out excess resin, and help in compaction. The manufactured cellular panels are displayed in Figure 4-13. Figure 4-13a shows the base design with periodic cells and Figure 4-13b shows the optimized design obtained through the parametric optimization approach featuring the hierarchical cellular arrangement.

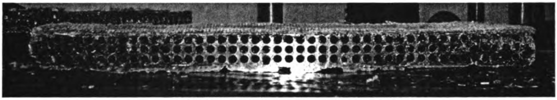

(a) Base design with periodic cells

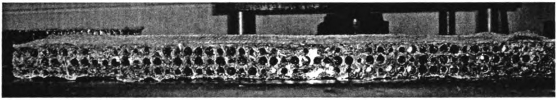

(b) Optimal design with hierarchical cellular arrangement

Figure 4-13. Manufactured base and optimal cellular biocomposite panels for case-study

4.4 Flexural Testing of VARTM Hierarchical Samples

The performance of the cellular panels manufactured for the case study was evaluated through flexural testing. This section introduces and discusses the testing procedure and setup, instrumentation, and loading scheme used.

Flexural testing was performed in such a way that the tests replicated the loading conditions experienced by a continuous panel system (i.e., a bridge deck). A schematic of a continuous panel system on multiple supports is shown in Figure 4-14a. The continuous panel system is assumed to be loaded in between supports, representing maximum loading conditions. Taking symmetry into consideration, the system can be reduced to a two-span panel arrangement as shown in Figure 4-14b. From the simplified system, the bending moment diagram demands are obtained as given in Figure 4-15a. In order to achieve the desired design moments shown in Figure 4-15b the panels were tested as a simply supported beam with a cantilevered overhang and the beam was loaded at the cantilever tip and at the middle of the span. The load levels at midspan and at the cantilever overhang were selected so as to match the desired design moment diagram. A schematic of the testing setup is shown in Figure 4-16. The test setup was realized by mounting a stiff support beam on a universal loading frame. The two loading points and their respective magnitudes were achieved by means of a loading spreader beam. A picture of the actual test setup is shown in Figure 4-17.

The test unit was loaded monotonically until failure at a loading rate of 0.01 mm/sec. The deflection of the samples was measured at both points of loading using externally mounted displacement transducers (Figure 4-16 and Figure 4-17). Four electrical resistance strain gages were mounted the tensile and compressive faces of the two maximum moment locations on regions of maximum tension and compression (Figure 4-16). The strain gage readings, external displacements, and applied load were simultaneously recorded with a digital data acquisition system.

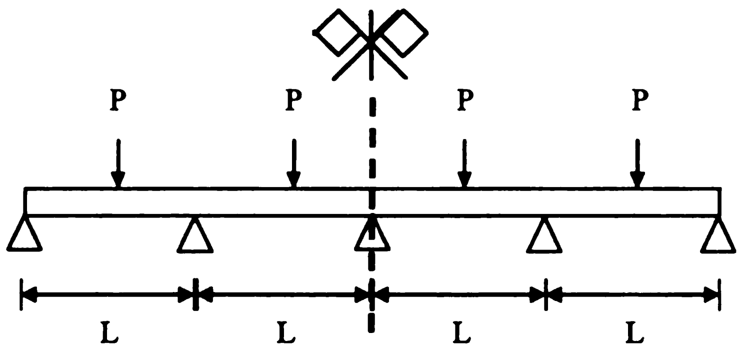

(a) Continuous panel system with multiple supports

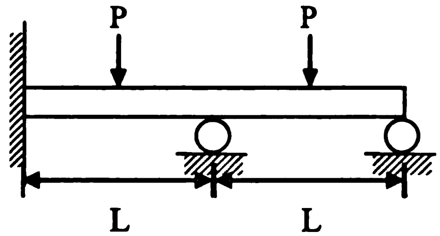

(b) Reduced two-span panel arrangement

Figure 4-14. Loading and boundary conditions of a simplified continuous panel system

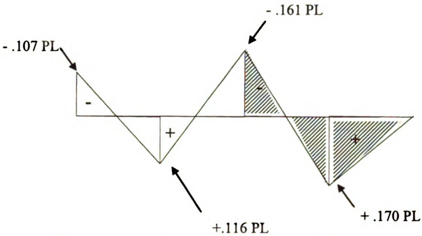

(a) Bending moment diagram of simplified continuous panel system

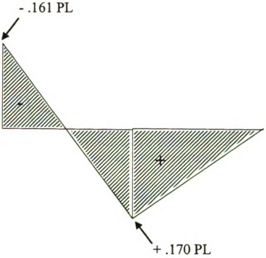

(b) Bending moment diagram on tested unit

Figure 4-15. Bending moment diagram to be replicated during testing

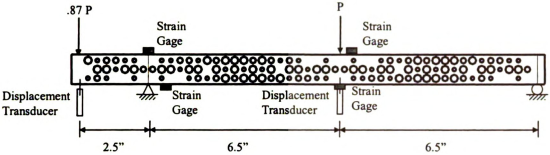

Figure 4-16. Schematic of testing setup

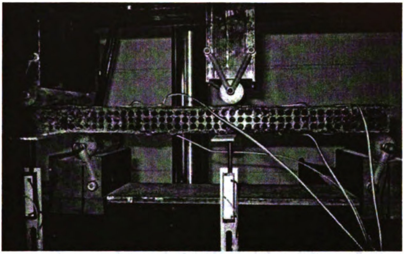

(a) Base design with periodic cells

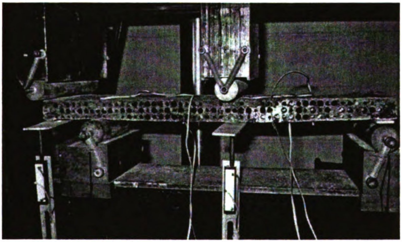

(b) Optimal design with hierarchical cellular arrangement

Figure 4-17. Picture of continuous beam test setups on universal loading frame

While the ultimate load capacity of both panels was similar (4% difference), their response was very different. The base non-optimal design was very flexible (Figure 4-18a) with large cell distortions while the response of the optimal design was essentially linear elastic exhibiting relatively small deformations (approximately 200% smaller at failure) (Figure 4-18b). Results obtained from the flexure tests and comparisons between the base and optimal structures obtained for the case study are discussed in detail in the following section.

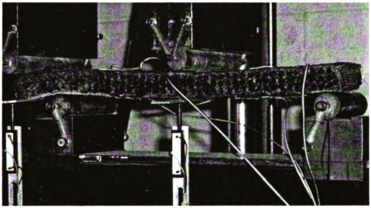

(a) Deformation of base design during testing

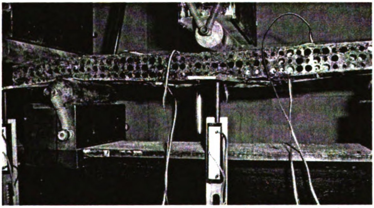

(c) Deformation of optimal design during testing

Figure 4-18. View of test unit response

4.5 Results and Discussion

This section provides the experimental results and comparison between the base and optimal structures obtained for the design case study of this thesis. The load-deflection responses of the jute/green-hemp/UPE cellular panels are shown in Figure 4-19 and Figure 4-20 for the base and optimized designs, respectively while a summary of results is given in Table 4-2. The response of the base design was much more flexible (200% higher) than the optimal panel with a compounded response that showed stiffening after significant deformations. Conversely, the response of the optimal panel was essentially linear elastic up to failure with comparatively smaller deformations (twice as small).

Both the base and optimal cellular structures failed due to tensile stresses at the peak moment zones. However, the base design had a tensile rupture under the positive moment region, at a peak load, *P*, of 0.43 kips. The optimal design failed in tension at the negative moment region at a peak load of 0.45 kips. Thus, the failure capacity of both designs was essentially the same, with the optimal design reaching a failure load that was only 5% higher than that of the base design.

The effect of the optimized material layout on the performance of the cellular biocomposite panels was much more evident in their deformation response. Figure 4-19 shows the central load (*P*)-displacement response for the base and optimal designs, while Figure 4-20 gives the edge load (.87*P*)-displacement response. The reason to display the load-displacement responses with respect to the load at either the midspan or at the cantilever tip is to distinguish the respective stiffnesses of the panel regions. As expected, the optimized design displayed a higher initial stiffness (i.e. the slope of the linear portion of the load-displacement response) and secant stiffness to maximum load at both midspan and the cantilever tip than the base design (Table 4-2). A schematich description of approach used to determine the initial and secant stiffnesses in Figure 4-21. Specifically, with respect to the central load, the optimal panel system was found to have an initial stiffness approximately 41% larger then the initial design and a 64% larger secant stiffness to maximum load. It should be noted, however, that the optimized design did have a 16% higher relative density than the base design. However, it is clearly the optimized material layout has the biggest influence in allowing this sample to have a significantly higher stiffness.

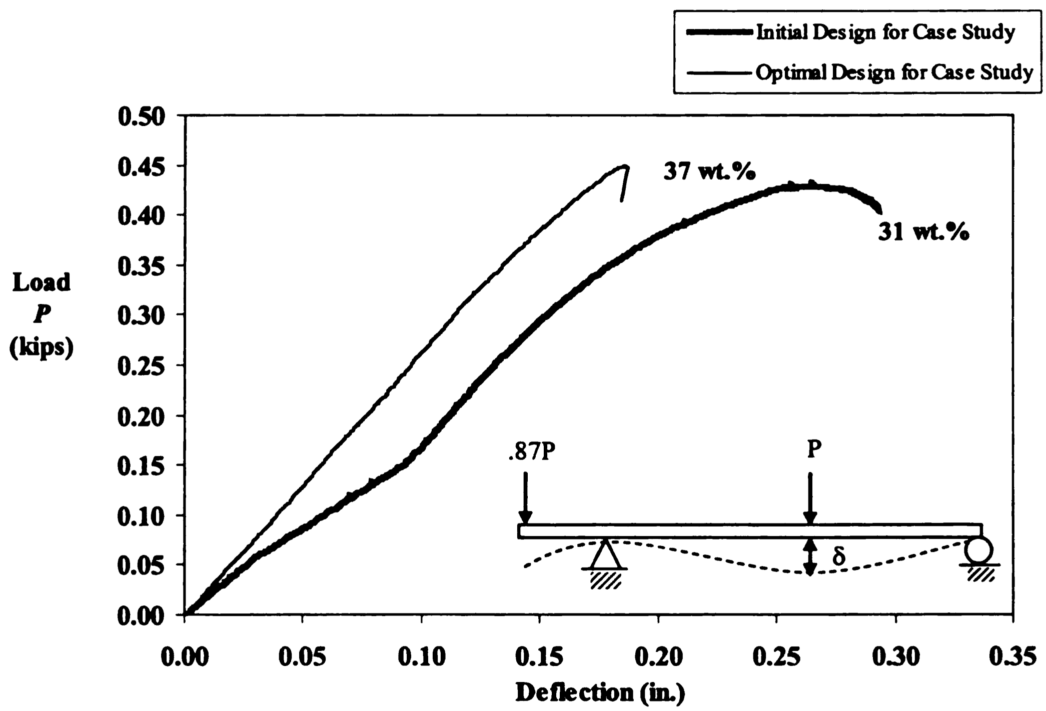

Figure 4-19. Force-displacement response at midspan

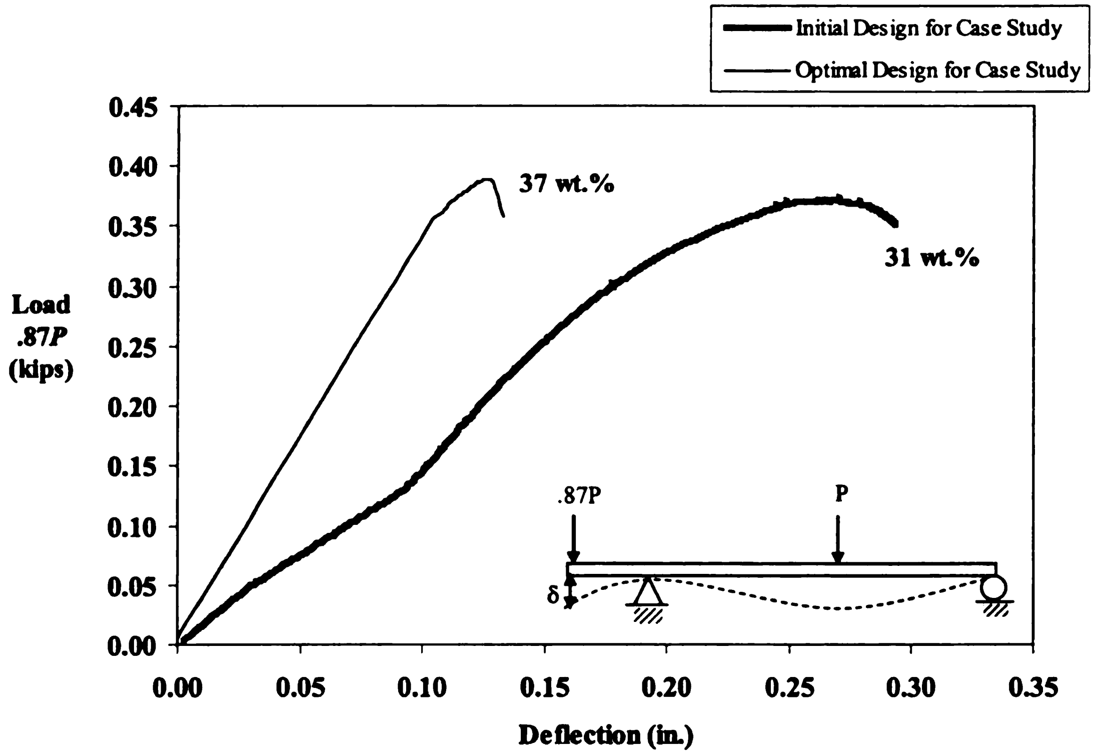

Figure 4-20. Force versus displacement response at cantilever tip

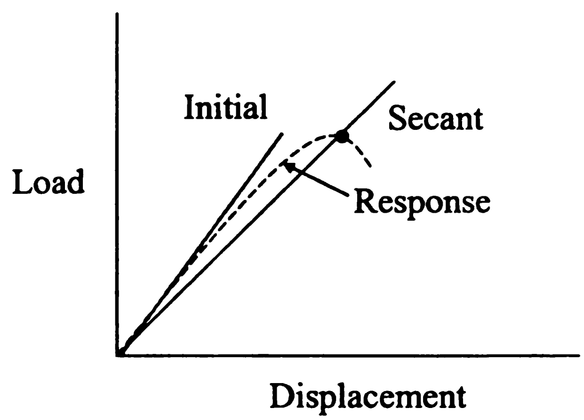

Figure 4-21. Initial and secant lines used to determine sample stiffnesses

Table 4-2. Flexural test results summary with respect to the central load

	Fibers by Wt.%	Strength (kips)	Initial stiffness with respect to central δ (kips/in)	Secant stiffness to Max. Load with respect to central δ (kips/in)	Initial stiffness with respect to edge δ (kips/in)	Secant stiffness to Max. Load with respect to edge δ (kips/in)
Initial Design	31	0.43	1.70	1.41	2.20	1.55
Optimal Design	37	0.45	2.40	2.31	4.15	3.07

The load-displacement behavior plots shown in Figure 4-19 and Figure 4-20 show that the test units has similar capacity, however, their response was markedly different. The optimal design exhibited essentially a linear response up to failure. Conversely, the base design showed two distinct nonlinear responses, the second one showing significant stiffening. This behavior is a result of shear distortion of the periodic cells in the base design. Shear deformations occur when a structure has few or no transverse diaphragms or internal bracing, so that the vertical shear force across a cell causes the internal bracing and webs to flex independently out-of-plane. This deformation is similar to that of a Vierendeel truss as shown in Figure 4-22a (Hambly 1991). The shear distortion of the Vierendeel truss can be minimized by addition of internal diagonal bracing as shown in Figure 4-22b, which is the well-known traditional design of truss structures. This same distortion may also be present in periodic cellular structures as illustrated in the cantilever beam with a tip load in Figure 4-23a. Cell distortion is not just resisted by out-of-plane flexure of the top and bottom slabs and webs but also by in-plane bending and shear of the plate elements. Cell distortion can be minimized by aligning the material such that the stiffness of the structure is maximized as shown in Figure 4-23b (Hambly 1991). It can be noticed that the rearranged material essentially follows the direction of inclined diagonal braces of a traditional truss. Not surprisingly, traditional topology optimization results (see Section 2.1.2) look like truss structures

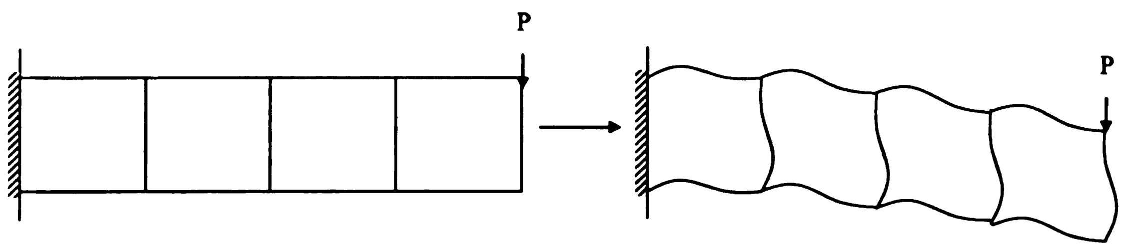

(a) Shear deformation

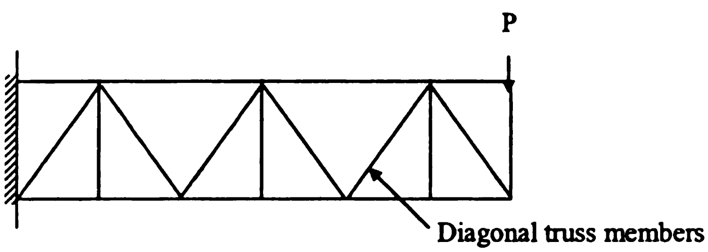

(b) Internal diagonal braces added to minimize shear deformations

Figure 4-22. Shear deformation of Vierendeel truss

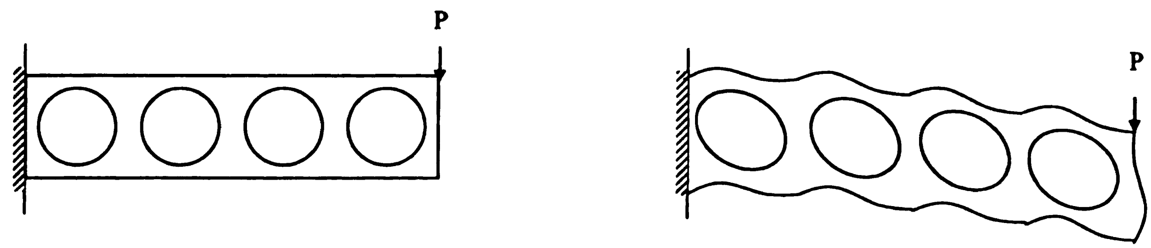

(a) Cell distortion

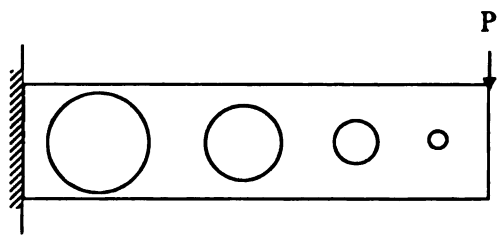

(b) Proper material alignment

Figure 4-23. Cell distortion in a cantilever beam with tip load

Periodic cells exhibit large distortion thus leading to a softer structure with slight nonlinear behavior. Through this shear distortion, the circular cells essentially ovalize in a deformation mode that requires little energy. However, once the cells "reorient" themselves, the material is aligned and thus more effective, leading to the stiffening branch of the response. By comparison, the linear response of the optimal design follows from the fact that the optimization procedure has essentially lead to a material layout that is already for the stiffest performance, i.e. without shear deformations. It can be further observed that upon "realignment" of the cells in the base design, the slope (i.e., stiffness) of the load-deformation response is initially equal (parallel) to that of the optimal design. Unfortunately, the base system later develops other areas of shear-dominated response leading again to softening behavior. It can thus be concluded that the response of the tested samples would correspond to the behavior of the Vierendeel truss, for the base design, and an actual triangulated truss structure for the optimal design (see Figure 4-22). Thus, the computationally optimized design essentially has arranged the material in a truss-like fashion, just as what is expected in results from traditional topology optimization approaches.

The strain behavior was also examined at four locations (see strain gage locations in Figure 4-16), which was different in comparison to the load-displacement response. Typical load-strain behavior is shown in Figure 4-24 through Figure 4-25. In these figures it can be seen that while the load-displacement response for the base design was highly nonlinear, all of the load-strain histories were essentially linear elastic. The reason is that the shear-induced deformations in the base design are a cross-sectional effect away from the critical sections, whose strain distribution continues to increase essentially in a linear way. The load-strain responses also show a stiffer response for the optimal design and the strains measured for the base design at failure were larger than for the optimal design. The only explanation for failure of the optimal design at a lower strain is material variability or manufacturing imperfections. This highlights the importance of implementing safety factors in the strain limit formulation of the design optimization problem.

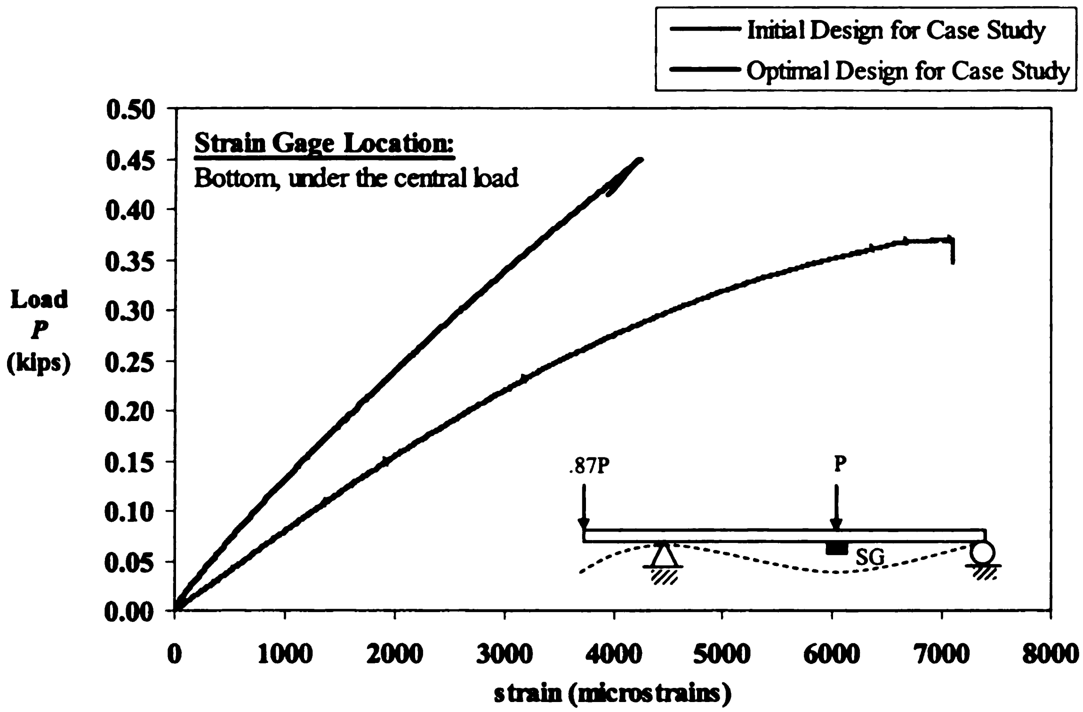

Figure 4-24. Load-strain response at extreme tension fiber on maximum positive moment section

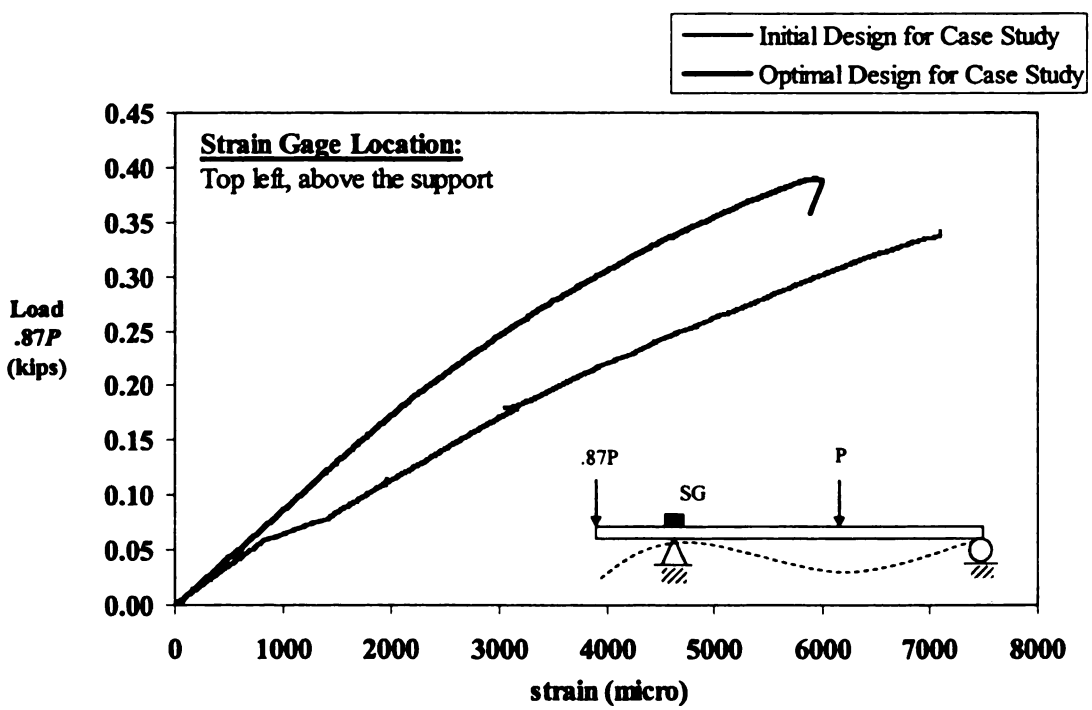

Figure 4-25. Load-strain response at extreme tension fiber on negative moment section

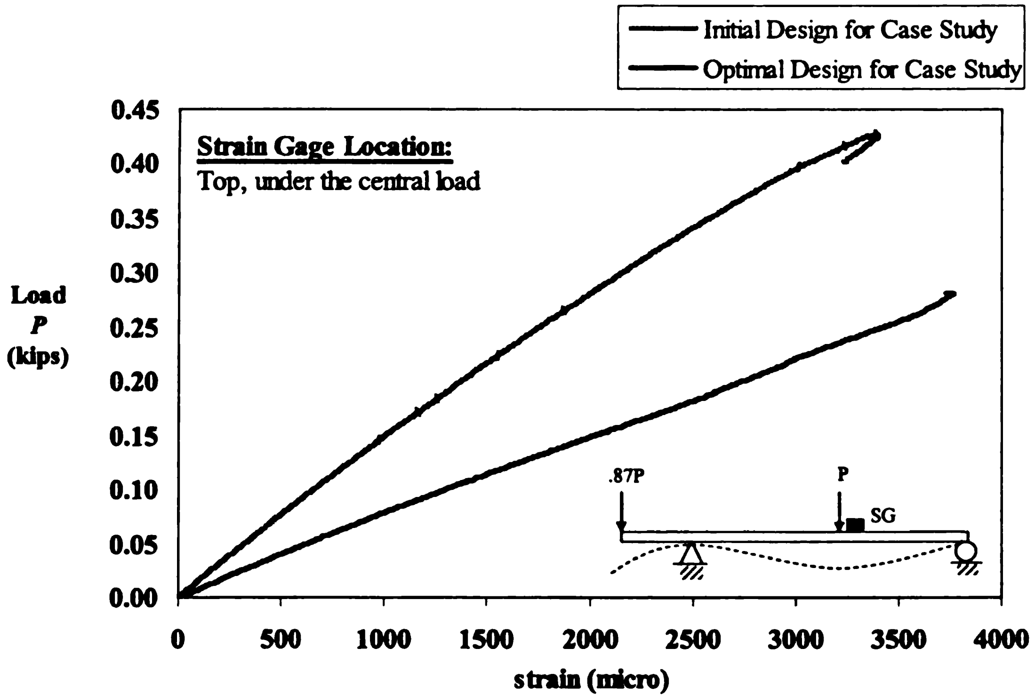

Figure 4-26. Load-strain response at extreme compression fiber on maximum positive moment section

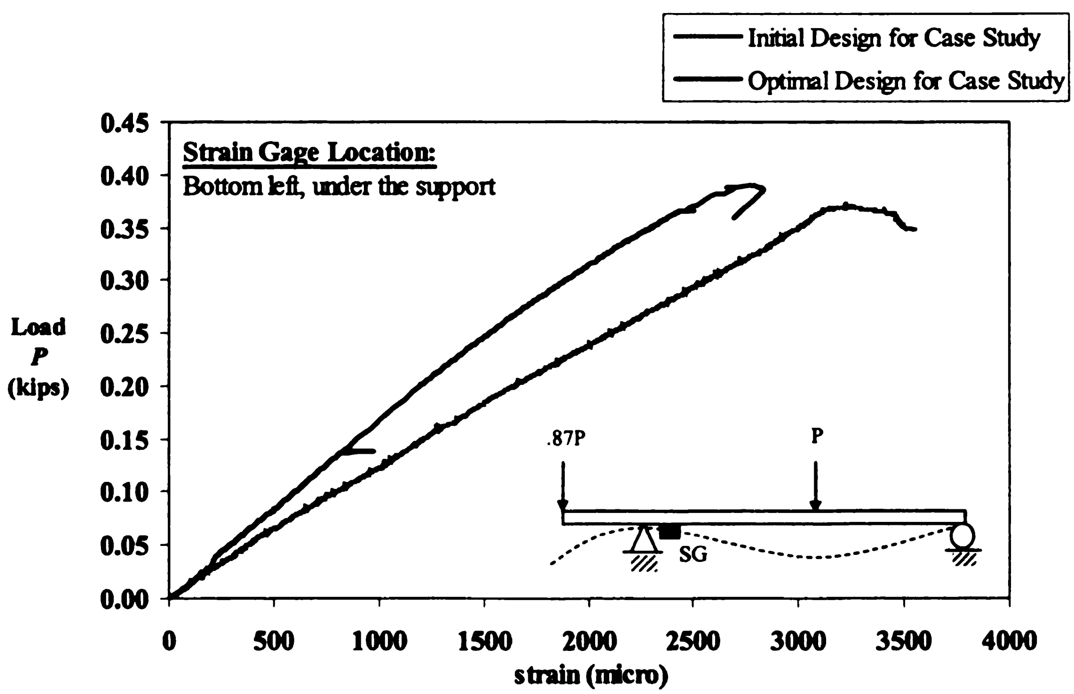

Figure 4-27. Load-strain response at extreme compression fiber on negative moment section

The initial stiffnesses obtained for both the base and optimal designs (see Table 4-2) were compared to those obtained through finite element analysis (FEA). The stiffnesses were obtained from FEA by taking the force/displacement at the location of the concentrated load. The deformations of the base and optimal designs obtained from the FE analysis are displayed in Figure 4-28 and Figure 4-29 below. Table 4-3 displays the comparison in computational and experimental initial stiffnesses. The findings show a 58% difference in the ratio of base to optimized stiffnesses. This difference could be due to the difference in the elastic modulus implemented in the FEM model and the actual modulus of the manufactured samples. Furthermore, unlike the manufactured samples, the FEM model was not created to include the hybrid jute mat/green-hemp design.

Upon close inspection of Figure 4-28, a slight distortion of the periodic cells can be noticed. As previously stated, the circular cells essentially ovalized (see Figure 4-23) until they were "reoriented". This reorientation assisted in aligning the material, thus creating a stiffer structure.

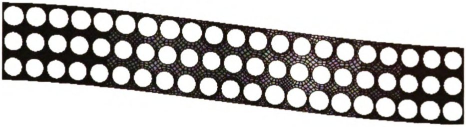

Figure 4-28. Deformation experienced by base design obtained for the case study

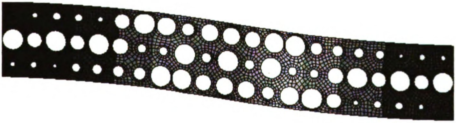

Figure 4-29. Deformation experienced by optimal design obtained for the case study

Table 4-3. Comparison in initial stiffness

	Experimental ratio of stiffness (k_E)	Computational ratio of stiffness (k_C)	k_E/k_C
$k_{base}/k_{optimal}$	0.71	0.45	58.0

5 CONCLUSIONS AND RECOMMENDATIONS

5.1 Conclusions

The results presented from the computational and experimental studies have reported that through the use of a finite parametric approach to structural optimization the material distribution within a given domain can be enhanced to improve the load-bearing capacity of components while simultaneously accounting for manufacturing. Specifically, the findings in this study have led to the following conclusions regarding obtaining optimal and "buildable" material distributions to enhance the properties of biocomposites for load-bearing components.

- A finite structural optimization technique can be implemented using a parametric modeling approach that combines robust optimization algorithms with finite element analysis through file scripting.
- The parametric modeling approach is capable of optimizing the material distribution of a structural component within a given domain while incorporating multiple objective functions and design constraints.
- Due to the use of finite geometrically defined features the proposed optimization technique is also capable of producing design solutions that account for manufacturing constraints.
- Homogeneous designs with optimized cellular herarchical configurations in the form of voids, or cells, are appropriate for biocomposite components due to the complexity in fabricating them in

geometrically detailed components or with aligned reinforcement designs.

- Vacuum assisted resin transfer molding (VARTM) is a practical technique for manufacturing biocomposite cellular samples.
- Material layout optimization techniques can obtain optimal cellular design solutions with multiple hierarchies to improve the mechanical properties and structural performance of biocomposites.
- The parametric approach to material layout optimization was chosen because it allowed for the definition of additional constraints and multiple objective functions. However, for the case study that was examined, the constraints did not control the design. Under these conditions the problem could have also been solved with the multiresolution approach proposed by Chellappa et al. 2004. Nonetheless, it should be realized that this might not always be the case for all problems, or problem formulations, i.e., when design constraints or multiple objectives may have a stronger influence in the resulting optimal design.

5.2 Recommendations for Future Work

Recommendations for future work based on the findings of this research are regarding both the computational and experimental studies. Future work for the computational portion of this study should focus not only on optimizing the material distribution within the domain but also the material and resin systems that are incorporated into the fabrication of biocomposites. Optimizing these systems may also contribute to improving the mechanical properties of biocomposites desired for structural applications. Future work in the experimental portion of this study involves the improvement in achieving the optimized structural layouts and progress in automated manufacturing techniques, such as the VARTM method, for the fabrication of large-scale cellular, hierarchical components.

5.2.1 Material Layout Optimization Techniques

The proposed parametric modeling approach to optimization is a viable technique for achieving optimal material layouts; however, in order improve this procedure to obtain components with enhanced structural performance, further research and development is necessary. A variety of geometric parameters for improved void/cell positioning should be explored for the material layout within a given domain. Instead of only relying on the size of a void, or cell, to alter the material layouts, void positioning and shape should also be included as a factor. Incorporating more geometric parameters may assist in producing a variety of unique design solutions; however, it may also lead to void overlapping and exceeding the pre-defined domain. To account for this problem, post-processing techniques can be explored to "correct" or enhance designs as they evolve throughout the optimization procedure.

Another enhancement to the material layout optimization procedure could be addressed through modeling the material systems. Hybrid designs could be included in the FEM models to check for performance enhancements. Furthermore, the exterior of each void, or cell could be assigned a different material property, simulating a synthetic or natural fiber wall lining which can also have a positive effect on the overall structure performance.

5.2.2 Optimization of Material and Resin Systems

Future work is necessary for biocomposite materials to examine the physical properties of the natural fibers and resin systems for fabrication. Properties such as flammability, degradation, and robustness of both the fiber and resin systems should be noted, for they are all important in structural applications. In addition to the study of the physical properties, cost effective fiber treatment methods should also be assessed for possible improvement of fiber-matrix adhesion, fiber sizing for resin, and processing of fibers (Vaia and Krishnamoorti 2002). Furthermore, studies should be implemented regarding the replacement of unsaturated polyester resin systems, with bio-based systems which are more environmentally friendly.

5.2.3 Design of Optimized Structural Layouts

After achieving a design with an optimal cellular, hierarchical distribution, it is necessary to prepare this design for fabrication. Future work is needed to examine the various possibilities of fabricating the obtained optimal cellular hierarchies. For example, hierarchical cells can be created using non-structural foams wrapped with synthetic or natural fiber composites or by lining the exterior of each void with a continuous composite material. These concepts may assist in enhancing the performance of cellular biocomposite panels and is a design technique that should be addressed in future work.

5.2.4 Improving VARTM Manufacturing

Based on the results from this experimental study, VARTM has proven to be a viable technique for the manufacturing of biocomposite cellular components. Future work is needed to allow for full-scale manufacturing of these components in order to ensure their feasibility for structural applications. Fabrication of biocomposites should be optimized to achieve load-bearing components with high fiber volume fractions efficiently and in minimal time such that production of mass quantities is possible. Manufacturing time could be minimized by using multiple resin and vacuum ports which will be more feasible to include when manufacturing large-scale components. Furthermore, in order for VARTM to be considered as a cost-effective manufacturing process for the proposed optimal biocomposite panels, it will be necessary to locate reusable and/or integrated materials for implementation of this technique.

5.3 Applications of Biocomposite Structural Components

Biocomposites do have environmental and health safety advantages over conventional structural materials and have proven to compete with E-glass FRP composites. However, further research and development is still required in order to ensure the use of biocomposites as structural components. With further development, biocomposites may be able of serving in applications ranging from civil structures, such as pedestrian bridges, decks, and housing or building flooring systems, to aerospace structures, such as fuselages, wing skins, and other integrated components.

REFERENCES

6 REFERENCES

Allaire G., Francfort, G., Bendsoe, M. "Topology design of structures." *Nato ASI Series E*, Vol. 227, 239-248.

Allinger, F., Müller, M., Puchinger, and S. (1996). "A New Approach for Sizing, Shape, and Topology Optimization." *SAE International Congress and Exposition*. Detroit, MI.

Arora, J. (1989), Introduction to Optimum Design, McGraw Hill International Editions, Singapore.

Barker, R., Puckett, J. (1997). Design of Highway Bridges. Wiley Interscience.

Bendsöe, M. and Sigmund, O. (2003), Topology Optimization – Theory, Methods, and Applications. Springer Verlag, Berlin.

Beyer, G. (2000). *University of Dortmund*. Department of Computer Science Homepage [online] Available: http://ls11-www.cs.uni-dortmund.de (Accessed February 2005).

Brouwer, W.D.(2000). "Natural Fibre Composites: Where can Flax Compete with Glass?" *SAMPE Journal*, Vol 36, 18-23.

Brouwer, W.D., Van Herpt, E.C..and, Labordus, M. (2003). "Vacuum Injection Molding for Large Structural Applications." *Composites*, Vol 34, 551-558.

Burgueño, R., Quagliata, M.J., Mohanty, A.K., Mehta, G., Drzal, L.T., and Misra, M. (2004), "Load-Bearing Natural Fiber Composite Cellular Beams and Panels" *Composites Part A*, Vol. 35, 645-656.

Burgueño, R., Quagliata, M.J., Mohanty, A.K., Mehta, G., Drzal, L.T., and Misra, M. (2005), "Hybrid Biofiber-Based Composites for Structural Cellular Plates" *Composites Part A*, Vol. 36, 581-593.

Canonaco, M., Loher, U., Esslinger, V., Weisse, B (1997). "Structural Optimization Methods." *Computer Aided Optimum Design of Structures V*, Vol 28, 381-389.

Chellappa, S., Diaz, A.R., and Bendsoe, M.P (2004). "Layout Optimization of Structures with Finite-Size Features using Multiresolution Analysis." *Structural and Multidisciplinary Optimization*, Vol. 26, 77-91.

Chou, H., Premkumar, G., and Chu, C. H. (2001). "Genetic Algorithm for Communication Network Design -An Empirical Study of the Factors that Influence Performance," *IEEE Transactions on Evolutionary Computation,* Vol. 5, 236-249.

Daves, L (1991). Handbook of Genetic Algorithms. Van Nostrand Reinhold, New York.

Gibson R.(1994). Principles of Composite Material Mechanics. McGraw Hill, New York, NY.

Gibson, L. Ashby, M. (1988). Cellular Solids: Structures and Properties. 1st Edition, Pergamon Press, Oxford, UK.

Goodman, E. (2002). GALOPPS User's Manual, version 3.2.4, East Lansing, MI.

Guervos, J. (1997). *University of Grenada*. Department of Architecture and Computer Technology [online] Available: http://kal-el.ugr.es/GAGS/gags-tutorial/node3.html) (Accessed February 2005).

Haftka, R., Gurdal, Z. (1993). Elements of Structural Optimization. Kluwer Academic Publishers.

Hambly, E. (1991). Bridge Deck Behaviour. Chapman & Hall, London, England.

Hepworth, D., Bruce, D. M., Vincent, J., and Jeronimidis, G. (2000). The Manufacture and Mechanical Testing of Thermosetting Natural Fiber Composites. *Journal of Materials Science* Vol 35, 293-298.

Hibbitt, Karlsson, Sorensen (2004) ABAQUS Users Manual, version 6.4, Pawtucket, RI.

Lackey, E., Vaughan, J., Inamdar, K., Hancock, B. (2004). "Statistical Characterization of Pultruded Composites with Natural Fiber Reinforcements." *Composites.* Tampa, Florida, October 6-8.

Lagaros, N. and Papadrakakis, K. (2002). "Structural Optimization using Evolutionary Algorithms." *Computers and Structures*, Vol. 80, 571-589.

Mattheck, C. (1997) DESIGN IN NATURE-Learning From Trees. Springer Publishing.

Mohanty, A.K., Misra, M., Hinrichsen, G. (2000), "Biofibres, Biodegradable Polymers, and Biocomposites: An Overview." *Macromolecular Materials and Engineering*, Vol.276/277. 1-24.

Olhoff, N., Bendsoe, M.P., and Rasmussen, J. (1991). "On CAD-Integrated Structural Topology and Design Optimization." *Computer Methods in Applied Mechanics and Engineering*, Vol. 89, 259-279.

Poli, R., Langdon, W.B. "Genetic Programming with One-Point Crossover and Point Mutation." *Proceedings of the Second International Conference on Genetic Programming*, 278-285.

Quagliata, M.J. (2003). "Development and Characterization of Biocomposite Cellular Beams and Plates for Load-Bearing Components". Michigan State University, East Lansing, MI. 1-200.

Red Cedar Technology (2004). HEEDS User's Manual, version 4.1, East Lansing, MI.

Rout, J., Misra, M., Tripathy, S.S., Nayak, S.K. and Mohanty, A.K. (2001). "The Influence of Fibre Treatment on the Performance of Coir-Polyester Composites." *Composites Science and Technology*, Vol. 61, 1303-1310.

Rozyany, G.I.N., Zhou, M., and Birker, T. (1992). "Generalized Shape Optimization without Homogenization." *Structural Optimization*, Vol 4, 250-254.

Sigmund, O. (2001). "99 Line Topology Optimization Code written in MATLAB." *Structural Multidisciplinary Optimization*, Vol 21, 120-127.

Sigmund, O., Tcherniak, D. (2001). "A Web-Based Topology Optimization Program." *Structural Multidisciplinary Optimization*, Vol 22, 179-187.

Spath, D., Neithardt, W., Bangert, C (2002). "Optimized Design with Topology and Shape Optimization." *Proceedings of the I MECH E Part B Journal of Engineering Mnaufacture*, Vol. 216, 1187-1191.

Srinivasan, A.V. (1995). "Smart Biological Systems as Models for Engineered Structures." *Material Science and Engineering*, Vol. 4, 19-26.

Turkkan, N. (2003). "Discrete Optimization of Structures using a Floating Point Genetic Algorithm." *Annual Conference of the Canadian Society for Civil Engineering*. Moncton, N.B., Canada, June 4-7.

Vaia, R. and Krishnamoorti, R. (2002). "Polymer Nanocomposites: Synthesis, Characterization, and Modeling." *American Chemical Society Conference*, Washington, D.C.

Verheus, A. (2002). *Centre of Lightweight Structures TUD-TNO*. Company Homepage. [online] Available: <http://www.clc.tno.nl/homepage.html > (Accessed April 2005).

Wall, M. (2001). *Mechanical Engineering at Michigan Tech.* Mechanical Engineering Homepage [online] Available: <http://lancit.mit.edu> (Accessed March 2005).

MICHIGAN STATE UNIVERSITY LIBRARIES
3 1293 02736 3567